227 (2023) 211826

Contents lists available at ScienceDirect

Geoenergy Science and Engineering

journal homepage: www.sciencedirect.com/journal/geoenergy-science-and-engineering

Multiple geological events controlling rock types development: A case study of Wufeng-Longmaxi formation in southern Sichuan Basin, China

Haoran Xie [a], Chao Liang [a,b,*], Jing Wu [c,**], Yingchang Cao [a,b], Yu Han [a], Yudi Liu [a], Zilong Zhao [a]

[a] School of Geosciences, China University of Petroleum (East China), Qingdao, 266580, China
[b] Key Laboratory of Deep Oil and Gas, China University of Petroleum (East China), Qingdao, 266580, China
[c] College of Earth Science and Engineering, Shandong University of Science and Technology, Qingdao, 266590, China

ARTICLE INFO

Keywords:
Geological events
Sedimentary environments response
Organic matter accumulation
Rock types development
Wufeng-longmaxi formation shales
Sichuan basin

ABSTRACT

During Late Ordovician to Early Silurian, global geological events such as volcanic activity, glaciation, and mass extinction affected sedimentary environments and organic matter (OM) accumulation, and controlled the development of organic-rich shales. Taking the Wufeng-Longmaxi Formation (WF-L Fm) shales in southern Sichuan Basin as the research object, based on the core, thin section and scanning electron microscopy (SEM) observations, combined with X-ray fluorescence (XRF) two-dimensional element distribution maps, X-ray diffraction (XRD), trace elements, carbon isotope composition and total organic carbon (TOC) data, the relationship between geological events and sedimentary environments, OM accumulation as well as rock types development are analyzed, and the sedimentary environments response to geological events is elaborated. Eight rock types have been identified, and the minerals occurrence model has been characterized. By using Cu content, Mo content, $\delta^{13}C$ and TOC to measure paleoproductivity, Sr content and Sr/Cu to judge paleoclimate, Sr/Ba to measure paleosalinity, and U/Th, V/Cr, V/Ni, and Ni/Co to analyze redox conditions, the sedimentary environments of the WF-L Fm shales can be furtherly divided into 7 intervals. In general, the deep water hypoxic-anoxic environments from Interval I to Interval V is conducive to the formation of organic-rich shales. The organic-rich shales formed in the anoxic environments from Interval I to Interval V are related to the fact that volcanic activities not only release a large amount of nutrients, promote biological prosperity and improve productivity, but also make the water in a sulfide anoxic environment, which is conducive to the preservation of OM. The rapid rise and fall of sea level caused by the Hirnantian glaciation harmed the living environments of organisms, led to the mass extinctions and provided material sources for OM accumulation, resulting in high TOC in the rock types of Interval IV. Irregular gravity flow can enhance terrigenous input in deep water for a short time and dilute OM, which is one of the reasons for the low TOC in the rock types of Interval VI to Interval VII. Upwelling current enhances nutrient flux in surface water and improves primary productivity of water, thus affecting the development of WF-L Fm organic-rich shales. Based on the aforementioned interpretations, the sedimentary model of the southern Sichuan Basin was established.

1. Introduction

The Late Ordovician to Early Silurian was an important global geological transition period, during which many global comparable geological events occurred, such as global volcanic events, glaciation, mass extinctions, and so on (Finnegan et al., 2011; Algeo et al., 2016; Lu et al., 2019; Yang et al., 2021). These geological events undoubtedly had important impacts on the sedimentary environments, which in turn affected the sediments and organic matter (OM) accumulation (Brenchley et al., 2003; Zou et al., 2018; Li et al., 2020). Volcanic ash and gas caused sulfurized anoxia environments in water bodies, volcanic ash clouds obscured the sunlight resulting in the decrease of surface temperature (Haeckel et al., 2001; Cooper et al., 2018). Meanwhile, the nutrients released by the hydrolysis of volcanic ash were beneficial to algae growth and reproduction (Duggen et al., 2007; Langmann et al., 2010; Olgun et al., 2013). The large-scale glaciers formed during the glacial period caused the sea level to fall and the water depth to become shallower, which made the Yangtze Sea in a relatively high oxygen

* Corresponding author. School of Geosciences, China University of Petroleum (East China), Qingdao, 266580, China.
** Corresponding author.
E-mail addresses: xiehaoran2016@163.com (H. Xie), liangchao0318@163.com (C. Liang), wujing6524982@163.com (J. Wu).

https://doi.org/10.1016/j.geoen.2023.211826
Received 26 May 2022; Received in revised form 8 April 2023; Accepted 18 April 2023
Available online 22 April 2023

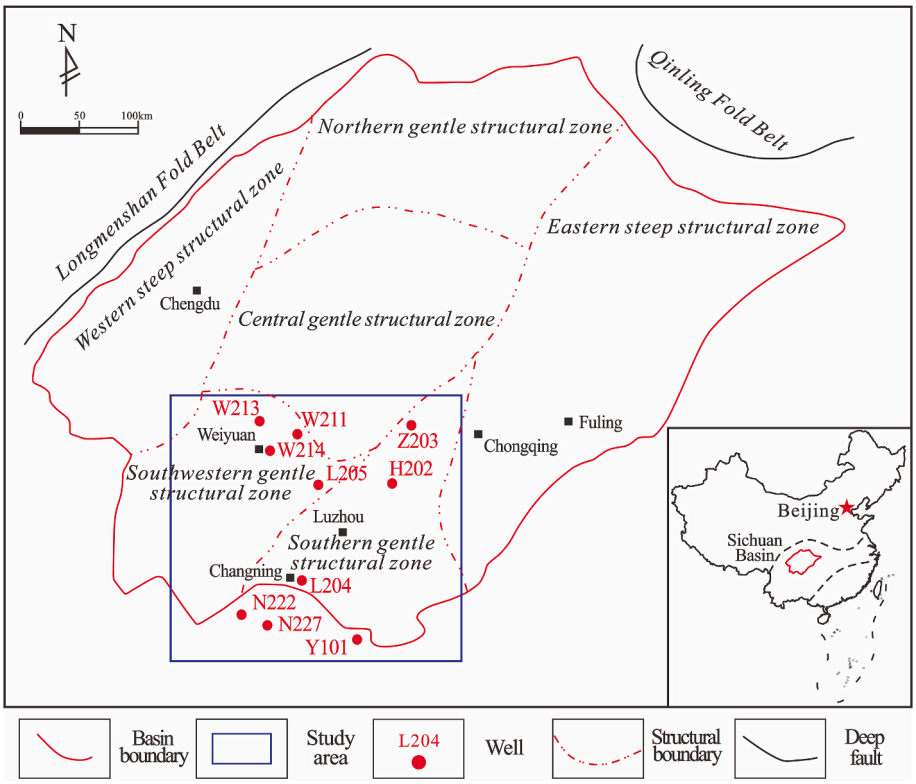

Fig. 1. Tectonic division and geographical location map of Sichuan Basin (modified from Yan et al., 2022; the tectonic division of the Sichuan Basin data comes from Wang et al., 2019b).

content environment during the glacial period and destroyed the preservation environments of organic-rich sediments (Hammarlund et al., 2012; Yan et al., 2012; Chen et al., 2021; Zhang et al., 2021). After the glacier melting, a large amount of fresh water was generated and injected into the ocean, which caused the sea level to rise significantly, and the water deepened and formed a stable anoxic environment conducive to the preservation of OM (Lambeck and Chappell, 2001). The mass extinctions provided material sources for the accumulation of OM, and the anoxic water environments formed by volcanic activity and glacier ablation made the enriched OM well preserved (Oman et al., 2005; Jones et al., 2017). With the increase of terrigenous material input, the content of sandy detrital material in sediments would increase, and the hydrodynamic environments would be more turbulent, which was not conducive to the preservation of organic matter in sediments (Wu et al., 2019b).

From the Late Ordovician to Early Silurian, superior marine source rocks of the Wufeng-Longmaxi Formation (WF-L Fm) were deposited in the southern Sichuan Basin because of two global transgressions (Zhao et al., 2016; Potter, 2018; Chen et al., 2021; Wang et al., 2021). Organic-rich shales of the WF-L Fm have strong heterogeneity (i.e., variations in mineral composition, sedimentary structure, element enrichment and OM content), which is the result of synergistic effects of sedimentary environments and sedimentary processes changes caused by specific geological events (Jiang et al., 2015; Liang et al., 2017; Hu et al., 2019; Wu et al., 2019a; Lu et al., 2019; Qiu et al., 2022; Wu et al., 2022). To clarify the sedimentary environments response to different geological events is the basis of shales sedimentary environments analysis, further elucidating the characteristics of rock types development and establishing a sedimentary model.

In this study, we selected the southern Sichuan Basin as the study area, systematically observed and identified the cores and thin sections, and examined the scanning electron microscopy (SEM) data, X-ray fluorescence (XRF) two-dimensional element distribution maps, X-ray diffraction (XRD) whole-rock mineral analysis, carbon isotope composition, and total organic carbon (TOC) data to describe the macro and microscopic characteristics of the rock types in detail, exploring their sedimentation processes. We also used the trace elements and geochemical indicators to reconstruct the paleo-sedimentary environments. The goals of this study is to explore the impacts of volcanic activity, glaciation, mass extinction and other geological events on the development of organic-rich shales in the Late Ordovician-Early Silurian, and clarify the mechanism of the influence of geological events on the development of rock types in southern Sichuan Basin and even on the global scale.

2. Geological setting

Southern Sichuan Basin is on the southwestern edge of the Upper Yangtze Platform and its main body is located in the southwestern gentle structural zone and the southern gentle structural zone of Sichuan Basin (Fig. 1; Zhao et al., 2017; Wang et al., 2019; Yan et al., 2022). During the Late Ordovician-early Silurian, the South China Block separated from Gondwana Continent and only attached to the northwest margin of Gondwana Continent, and the South China plate is composed of Yangtze and Cathaysia blocks (Zhang et al., 2013; Ge et al., 2019; Yang et al., 2020; Xiao et al., 2021). The Yangtze block merged with the Cathaysia Block to form the Cathaysia Old Land, and then the Cathaysia Old Land continued to expand to the northwest, forming the Central Guizhou Uplift and Hunan-Hubei Uplift in the southern margin of the Upper Yangtze region (Zhang et al., 2013; Gong et al., 2017; Dong et al., 2019; Liu et al., 2022). The main sedimentary area of the Yangtze block was surrounded by Chuanzhong Uplift, Central Guizhou Uplift and Kangtien Old Land, forming a semi-restricted shallow sea basin, which developed a deep water environment of stagnant flow and anoxia, and deposited a set of black siliceous shale and mudstone (Zou et al., 2010; Yang et al., 2016; Li et al., 2019; Fan et al., 2020).

The Yangtze Block was located near the equator during the Late Ordovician (Torsvik and Cocks, 2018; Zhang et al., 2019; Liu et al.,

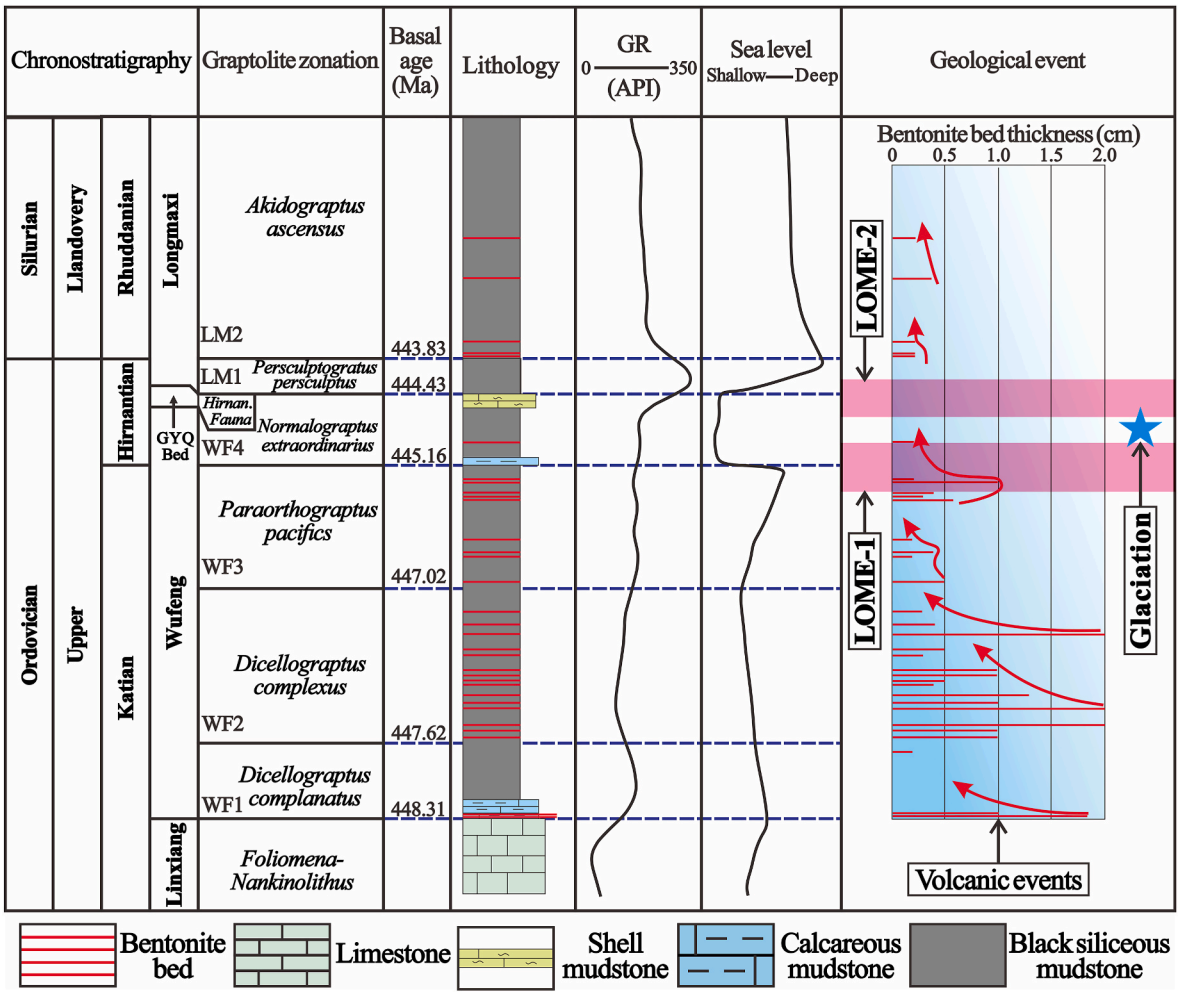

Fig. 2. Stratigraphy of the WF-L Fm in the Sichuan Basin (modified from Lu et al., 2022; sea level data comes from Zhu et al., 2021).

2022). The warm and humid climate makes weathering effect strong, producing a large number of debris substances and clay substances, and deposits thick WF-L Fm shales (Xi et al., 2019; Zhao et al., 2022). The WF-L Fm shales are underlain by thick, shallow Ordovician marine limestone and capped by mid-Silurian Luoreping Formation light gray to yellow siltstone (Fig. 2; Liang et al., 2012; Ran et al., 2015; Feng et al., 2021; Zhu et al., 2021). A large number of volcanic ash layers in the Wufeng Formation and lower part of the Longmaxi Formation imply that volcanic activities were frequent in these deposition periods. Although the volcanic activity tended to diminish during the deposition period of the Longmaxi Formation, its influence still existed (Lu et al., 2021).

3. Data and methods

For this research, we collected the data from 10 wells within the southern Sichuan Basin (Well H202, Well L204, Well L205, well N222, Well N227, Well W211, Well W213, Well W214, Well Y101, and Well Z203, locations see Fig. 1B). For observations and tests, a total of 126 well-core samples were collected from the target interval of the WF-L Fm shales.

Thin sections were prepared at a thickness of 0.03 mm, and the optical observations were performed using a Zeiss microscope (Axio Imager A2m) (Table 1). The mineralogical characteristics observations were performed on platinum-coated, thin sections by using a Scanning electron microscope (Zeiss Crossbeam 550), and the samples for SEM observations were platinum-coated. The XRD analyses were conducted using an X-ray diffractometer (Panalytical X'Pert PRO) comprising a copper source, 40 kV operating voltage, and 40 mA measuring current, the measurement angle range was 5°–70° (Table 1). The XRF two-dimensional element distribution samples were conducted using a high performance micro area X-ray fluorescence spectrometer (BrukerM4 TORNADO) comprising 50 kV operating voltage, 600 μA measuring current, and 25 μm dot distance(Table 1). Samples were also analyzed for trace element content, carbon isotope composition, and TOC. The trace element content analyses were conducted using a plasma mass spectrometer (NexION 300D). The ambient temperature was 22.3 °C and the humidity was 19%. The carbon isotope composition analyses were conducted using a gas isotope mass spectrometer (MAT-253) (Table 1). The TOC analyses were conducted using a total organic carbon analyzer (LECO CS744) by inducing sample combustion in an O_2 atmosphere to convert total organic carbon to CO_2 (Wu et al., 2019b). Among them, the optical observations, the SEM observations, the TOC analyses, and the XRF two-dimensional element distribution analyses were conducted at the Key Laboratory of Deep Oil and Gas, China University of Petroleum (East China), and the trace element analyses, the XRD analyses, and the carbon isotope composition analyses were conducted at Beijing Research Institute of Uranium Geology.

4. Results

4.1. Petrological characteristics

According to the well core characteristics, thin section and SEM observation, and XRD analyses data, the mineral composition and

Table 1
Main analytical methods of samples from wells in southern Sichuan Basin.

Analytical item	Analytical processes	Instruments	Samples quantity
Optical observations	The 0.03 mm thick thin sections was placed on the loading platform, pressed and focused, Zeiss microscope observation (Axio Imager A2m) was used to record the observations, and the microscope camera is Axiocam 506 color.	Zeiss microscope (Axio Imager A2m)	126
SEM observations	The surface of the sample was polished by an argon ion polishing machine (Gatan 685) and coated with platinum film. After completion, the sample was put into a scanning electron microscope (Zeiss Crossbeam 550) for observation. The usual magnification is 1000–5000 times, and the maximum magnification is 400,000 times.	Argon ion polishing machine (Gatan 685)、Scanning electron microscope (Zeiss Crossbeam 550)	20
XRD analyses	5 g rock powder (200 mesh) was loaded into the groove of the XRD sample table and the surface was pressed flat with plate glass to avoid the preferred crystal orientation. X-ray diffractometer (Panalytical X 'Pert PRO) was used for testing, XRD patterns were obtained, HighScore Plus was used for qualitative processing and then K-value method was used for quantitative processing of minerals.	X-ray diffractometer (Panalytical X'Pert PRO)	17
XRF two-dimensional element distribution	Polish the surface of the sample to be tested, keep it flat, and keep the sample surface dry. Keep the surface level in X-ray fluorescence spectrometer (BrukerM4 TORNADO), and scan after vacuuming. Generally, single point scanning time is set at 3–5 ms, and point spacing is 30–35 μm. After scanning, the target element or element combination is selected to obtain the two-dimensional distribution diagram of the element or element combination.	X-ray fluorescence spectrometer (BrukerM4 TORNADO)	20
Trace element content	Weigh 500 mg of rock powder (200 mesh) and place in an oven (105 °C) for 2 h. Then cool it to room temperature. The 100 mg sample was weighed and added into the microwave digestion tank with 2 ml HF, 2 ml HCI and 6 ml HNO_3. After 20 min reaction, the sample was heated to 185 °C for 45 min digestion according to the microwave digestion procedure, then transferred to the acid catcher (160 °C) for 90 min, and then transferred to the 50 ml plastic quantitative tube for constant volume. Let it stand overnight and take the supernatant to be measured. A plasma mass spectrometer (NexION 300D) was used to determine the content of trace elements.	Plasma mass spectrometer (NexION 300D)	17
Carbon isotope	10 mg of rock powder (200 mesh) was placed in a weighing bottle and dried in an oven (100 °C) for 4 h. The treated samples were put into a headspace bottle, and the air in the headspace bottle was purged with high purity helium gas (purging for 10 min). After that, phosphoric acid was added for a full reaction for 20 h, and constant temperature of 25 °C was maintained throughout the whole process. After that, gas isotope mass spectrometer (MAT-253) was used for testing.	Gas isotope mass spectrometer (MAT-253)	17
TOC analyses	Weigh 140–150 mg of rock powder (200 mesh) into a carbon-sulfur analysis crucible. Firstly, use 10% hydrochloric acid solution by volume fraction to remove inorganic carbon (carbonate mineral), and then wash the remaining hydrochloric acid in the crucible with distilled water. The samples were dried in an oven hood for 8 h and then in an oven (60 °C) for 2 h. The samples were then analyzed using a carbon and sulfur analyzer (LECO CS744).	Carbon and sulfur analyzer (LECO CS744)	109

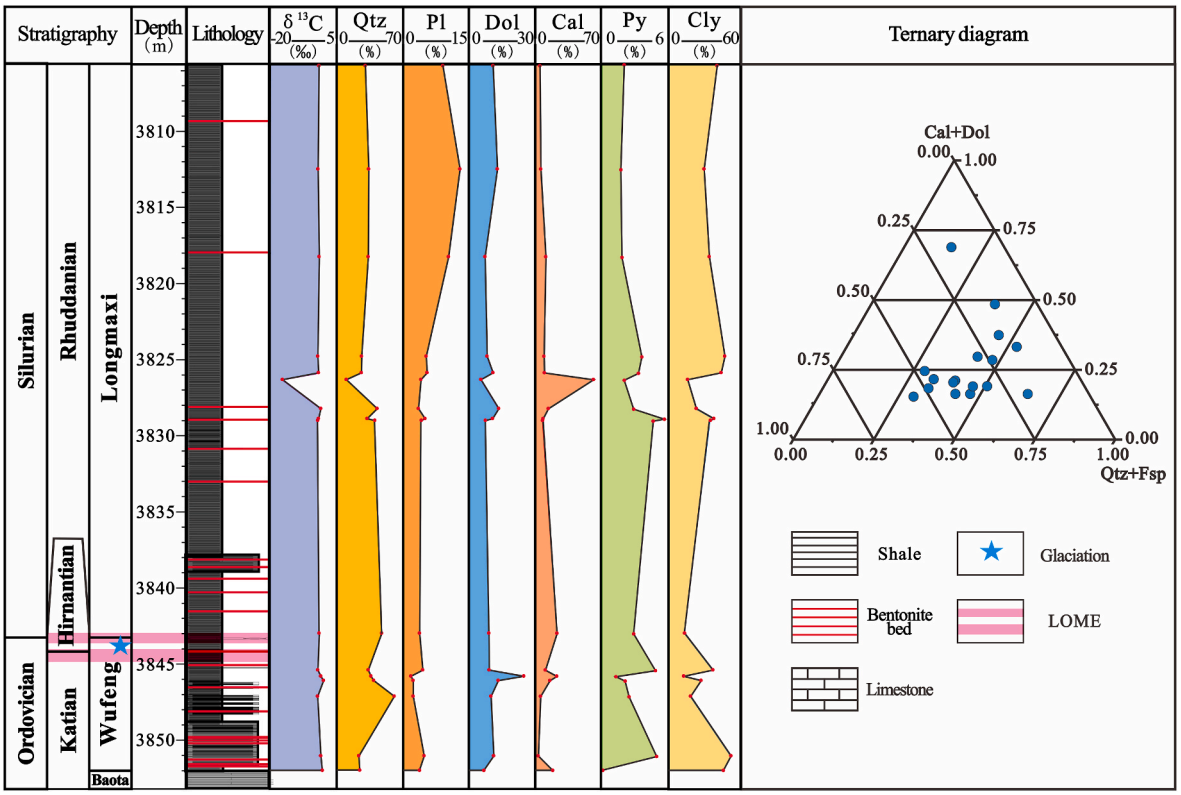

Fig. 3. Main mineral content of fine-grained sedimentary rocks from Well L204 in southern Sichuan Basin Abbreviations: Qtz-Quartz, Pl-Plagioclase, Fsp-Feldspar, Dol-Dolomite, Cal-Calcite, Cly-Clay mineral, LOME-The Late Ordovician mass extinction.

sedimentary structure characteristics of the fine-grained sedimentary rocks of the WF-L Fm are described in detail, which lays a foundation for the rock types classification.

4.1.1. Mineral composition

The WF-L Fm fine-grained sedimentary rocks are mostly grayish-black to black in the hand specimens. Among the 109 TOC analysis data obtained in the study area, the overall average TOC value was 3.73%, among which there were 70 samples with TOC exceeding 3%, mostly concentrated in 3%–5.5% (60 samples, average:4.33%). The main mineral components of the shales are clay minerals, quartz, calcite, dolomite, feldspar, and pyrite (Fig. 3), primarily the clay minerals and quartz (Fig. 3). The clay mineral content ranges from 12.90% to 52.20% (average: 31.36%). Illite is the dominant clay mineral species (Fig. 4A); a small amount of kaolinite and chlorite is also present. The quartz content ranges from 10.20% to 60.70% (average: 34.20%), including terrigenous quartz (Fig. 4B), biological quartz (Fig. 4C), and authigenic quartz (Fig. 4D). The feldspar content is from 1.80% to 15.80% (average: 5.44%). It is mainly composed of plagioclase, with a small amount of potassium feldspar (Fig. 4E). In general, the content of felsic minerals is the highest, accounting for 14.30%–63.00% (average: 39.64%). Carbonate minerals are mainly calcite (Fig. 4F), whose content is 3.30%–62.00% (average: 14.83%); the second abundant carbonate mineral is dolomite (Fig. 4G), whose content is 5.50%–24.90% (average: 11.22%). The overall content of carbonate minerals ranges from 14.60% to 67.50% (average: 26.05%). The shales also contain a small amount of pyrite, whose content is generally less than 5.00% (average: 3.14%), including idiomorphic pyrite (Fig. 4H) and framboidal pyrite (Fig. 4I).

4.1.2. Sedimentary structures

The WF-L Fm fine-grained sedimentary rocks are mainly developed with laminated structures and massive structures, with a few concretionary structures and bioturbation structures. The laminae can be classified into 4 types: clay-rich laminae, silt laminae, calcite laminae, and biosiliceous laminae. The clay-rich laminae are dark in color, and their mineral components are dominated by clay minerals, followed by quartz and calcite. The mineral particles are sub-angular to sub-rounded, with a diameter of less than 30 μm (Fig. 5A2). The silt laminae with mixed detrital grains have light colors, and quartz is dominated mineral. The detrital grains are in point contact or line contact, and the lamina thickness is 100–500 μm (Fig. 5A2). The calcite laminae are pure white on the core, a distinct and easy-to-recognize feature; they are developed as layers of columnar calcite, usually intercalated with a small amount of black clay material (Fig. 6B2). The biosiliceous laminae exhibit a grayish-white color, with visible biological fossils such as radiolarians and algae (Fig. 5C2). The massive structures have a grayish-white color on the cores, and are mainly composed of evenly distributed clay minerals, quartz, and feldspar. The concretionary structures are mainly developed in parallel between the silt laminae, bending the laminae above and below the concretion.

4.2. Rock types and characteristics

By systematically analyzing the core and thin-section samples and examining the SEM data, combined with the mineral compositions and content, XRF two-dimensional element distribution images and results of previous studies (Liang et al., 2012; Wang et al., 2020; Feng, 2019, 2022), the WF-L Fm shales can be classified into 4 categories: mixed fine-grained sedimentary rocks, siltstones, limestones, and claystone. Then, according to the sedimentary structures and characteristic minerals, the WF-L Fm shales can be subdivided into 8 rock types.

4.2.1. Laminated siliciclastic mixed fine-grained sedimentary rocks (RT1)

RT1 is the most common and widely distributed rock type in the WF-L Fm. The core is grayish-white and significantly hard (Fig. 5A1). The rock types are developed with laminated structures, assemblages of

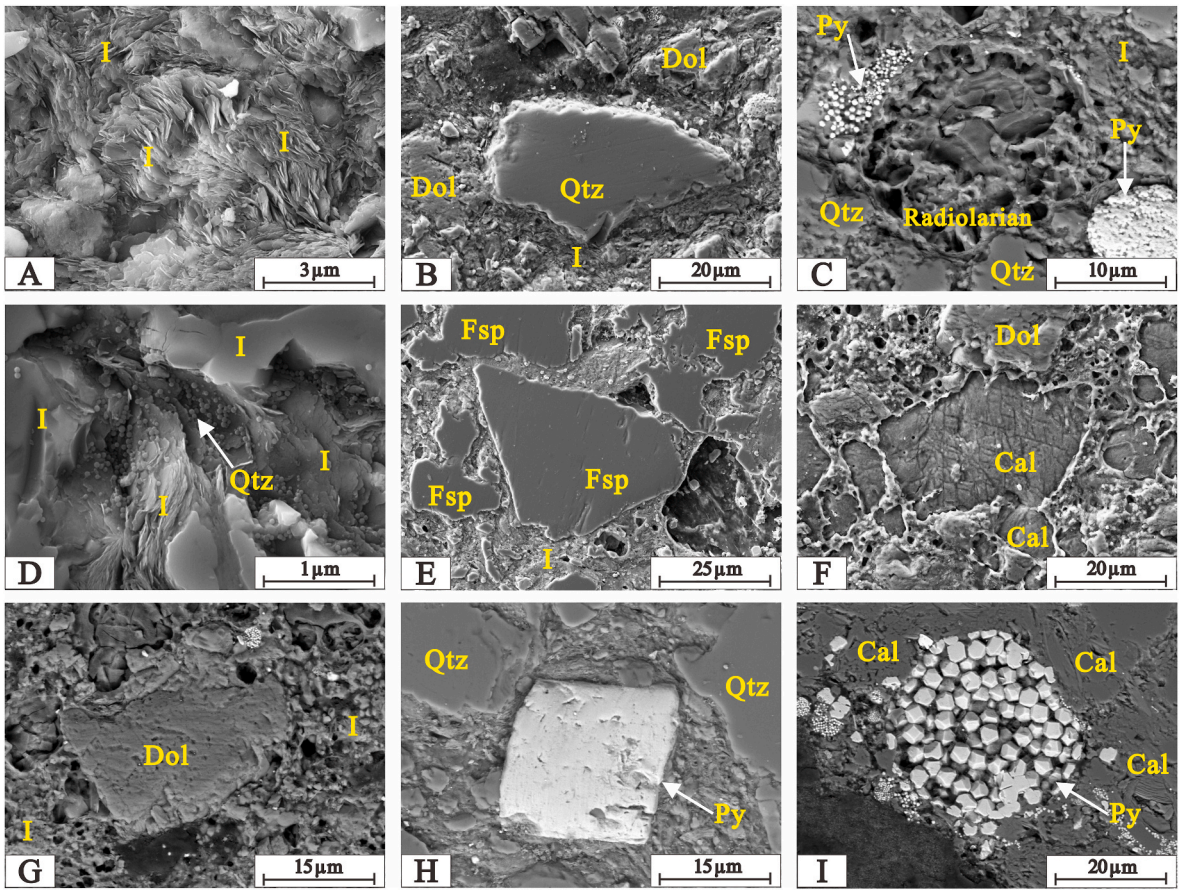

Fig. 4. Occurrence of various minerals in WF-L Fm shales in southern Sichuan Basin A. Illite (SEM), Well L204, 3851.86 m; B. Terrigenous quartz (SEM), Well L204, 3805.75 m; C. biological quartz-radiolarian (SEM), Well L204, 3845.45 m; D. Authigenic quartz (SEM), Well L204, 3843.37 m; E. Feldspar (SEM), Well L204, 3851.97 m; F. Calcite (SEM), Well L204, 3839.34 m; G. Dolomite (SEM), Well L204, 3839.34 m; H. Idiomorphic pyrite (SEM), Well L204, 3851.97 m; I. Framboidal pyrite (SEM), Well L204, 3838.40 m. Abbreviations: Qtz-Quartz, Fsp-Feldspar, Cal-Calcite, Dol-Dolomite, Cly-Clay mineral, Py-Pyrite, I-Illite.

Table 2
Main rock types of fine-grained sedimentary rocks from Well L204 in southern Sichuan Basin.

Rock types	Mineral content						TOC/%
	Qtz/%	Fsp/%	Cal/%	Dol/%	Py/%	Cly/%	
RT1	26.30 – 40.40 33.08	1.80 – 12.20 5.97	5.00 – 22.90 10.85	7.40 – 24.90 11.67	1.40 – 5.70 3.25	12.90 – 47.00 34.57	0.80 – 5.48 3.18
RT2	23.4 – 39.10 29.57	2.30 – 5.50 4.20	3.30 – 15.7 9.63	11.00 – 13.40 11.90	2.20 – 5.00 3.53	27.30 – 52.2 41.17	3.61 – 4.43 3.99
RT3	33.30	4.50	10.90	9.20	4.90	37.20	5.18
RT4	41.50 – 42.70 42.10	2.40 – 3.50 2.95	14.00 – 19.50 16.75	13.60 – 16.90 15.25	2.70 – 3.00 2.85	17.00 – 23.20 20.10	3.81 – 4.38 4.10
RT5	33.90 – 60.70 47.33	2.30 – 15.80 7.30	5.80 – 23.10 11.60	9.10 – 12.90 10.70	1.80 – 2.60 2.47	13.60 – 29.70 20.60	1.32 – 4.33 3.24
RT7	10.20	4.10	62.00	5.50	2.10	16.10	1.53
RT8	24.50	4.00	16.90	7.70	5.00	46.90	0.68

$\frac{26.30 - 40.40}{33.08} = \frac{\text{Min} - \text{Max}}{\text{Average}}$

Abbreviations: Qtz-Quartz, Fsp-Feldspar, Cal-Calcite, Dol-Dolomite, Cly-Clay mineral.

light-colored mixed silt laminae and dark clay-rich laminae, and occasionally developed with concretionary structures (Fig. 5A2). The mineral composition mainly includes clay minerals, quartz, calcite, dolomite, and feldspar (Fig. 5A3). Clay minerals and quartz are the dominant components (Table 2), whose average content is 34.57% and 33.08%, respectively. The quartz grains are 30–60 μm in diameter, angular to sub-angular. The feldspar grains are 20–45 μm in diameter, sub-angular to sub-rounded. The overall content of felsic minerals is relatively high, with an average of 40.92% (Fig. 7A). Calcite and dolomite are present, with particle sizes less than 40 μm, sub-angular to sub-rounded. The average content of calcite is 10.85%, and that of dolomite is 11.67%.

4.2.2. Massive siliciclastic mixed fine-grained sedimentary rocks (RT2)

RT2 is mainly developed in the lower part of the WF-L Fm, with small deposition thickness; they have a pelitic texture and are weakly stratified, showing a grayish-white to grayish-black color (Fig. 5B1). Clay minerals are their dominant mineral components, with an average content of 39.40% (Fig. 5B2). The content of detrital particles is relatively small and mainly quartz, calcite, and dolomite (Table 2). The

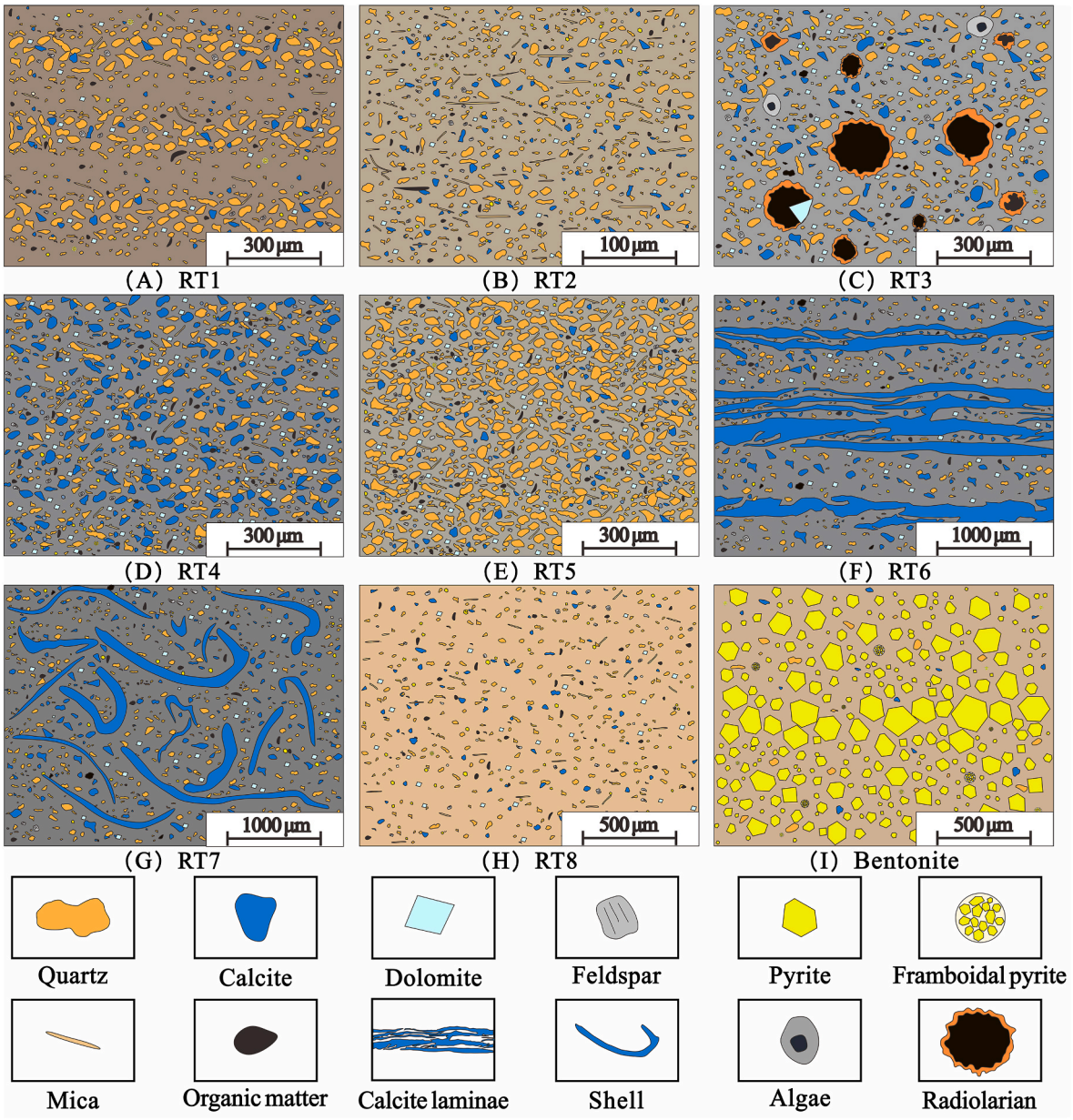

Fig. .7. Mineral occurrence of fine-grained sedimentary rocks for the WF-L Fm in southern Sichuan Basin.

quartz has a particle size of less than 30 μm and an average content of 29.57%, with sub-angular to sub-rounded grains (Fig. 5B3). The calcite has an average content of 9.63%, with sub-angular particles of about 20 μm in diameter. The dolomite is mostly micritic, with an average content of 11.90%. A small amount of mica is also present, with a particle length of 15–50 μm. The mica particles are short strip-shaped, severely fragmented, and scattered in the rock formations (Fig. 7B).

4.2.3. Laminated biosiliceous mixed fine-grained sedimentary rocks (RT3)

RT3 has laminar distribution in the lower part of the WF-L Fm, with high TOC content and a thickness varying from 0.2 to 1 cm. The rock type above and below them is RT2, with abrupt contacts. The core exhibits a gray or grayish-white color, with bedding structures (Fig. 5C1). Abundant siliceous organisms can be seen under the microscope, mainly radiolarians and sponges. The radiolarians have a yellowish-brown color and various shapes with a clear siliceous ring-shaped body structure (Fig. 5C2), randomly distributed in the rock type. Radiolarian's content is about 10.00%, with a particle size of 30–80 μm, mostly around 50 μm. Clay minerals are the dominant mineral components (Fig. 5C3), with a content of about 37.20%. The detrital material is mainly quartz, which is sub-angular, with a particle size of less than 30 μm, mostly mixed with the clay minerals and OM. The content of carbonate minerals is low, mostly calcite and dolomite. The calcite is in the form of detrital particles, with content of approximately 10.90% and a particle size of less than 25 μm. The calcite appears as well idiomorphic crystals with a content of 9.20% and a particle size of mostly 80–120 μm, filling in the radiolarian cavities (Fig. 7C).

4.2.4. Massive calcareous mixed fine-grained sedimentary rocks (RT4)

RT4 is mainly developed in the lower part of the Longmaxi Formation (Fig. 5D1), with high OM content (Table 2). They are mostly grayish-brown or grayish-black, with a pelitic texture (Fig. 5D2). The detrital materials are locally aggregated in point contact with a silty texture. The dominant mineral component is quartz, with a particle size of less than 30 μm and an average content of 42.10%, and the grains are sub-angular to sub-rounded. Clay minerals are the second most abundant, with an average content of 20.10%. The carbonate minerals are mainly calcite, followed by dolomite (Fig. 5D3). The particle size of

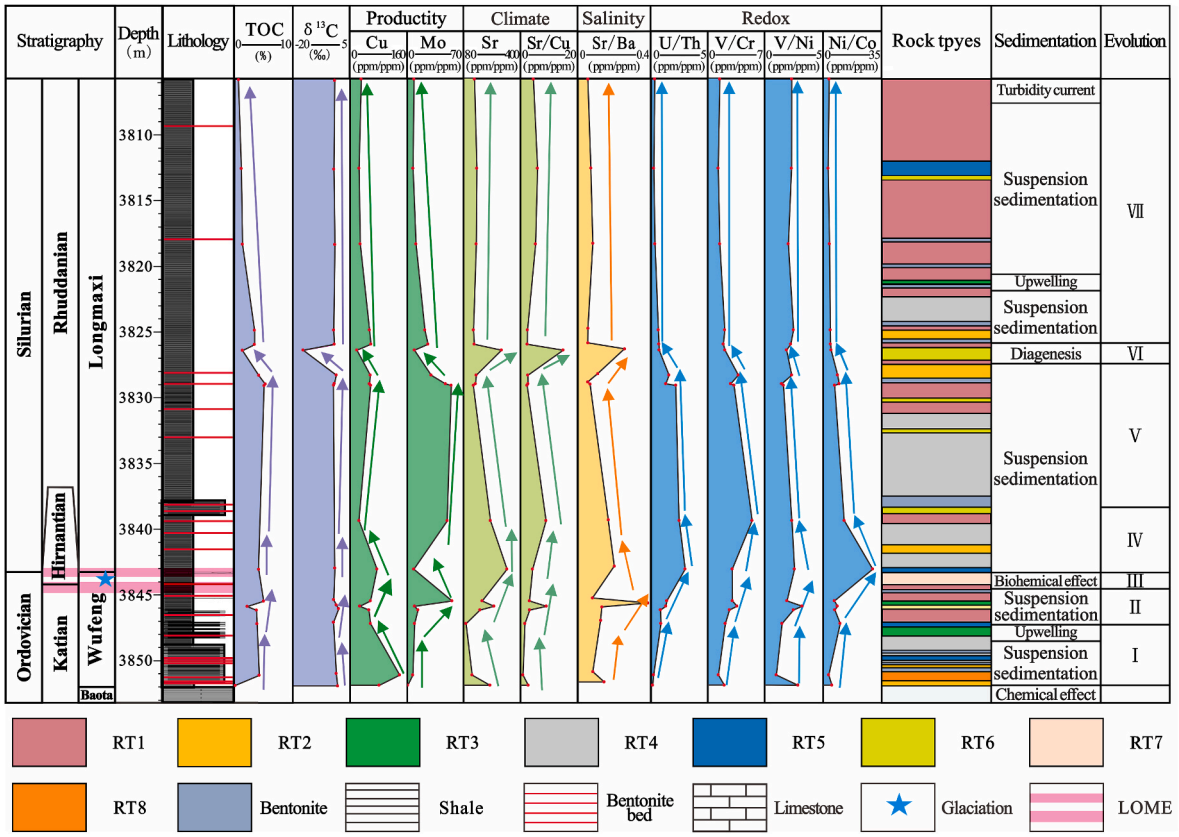

Fig. 8. Sedimentary environments evolution of Well L204 in southern Sichuan Basin.

calcite is less than 40 μm, and its average content is 16.75%, with sub-angular to sub-rounded grains. The dolomite grains are mostly well idiomorphic, with a diameter of 10–40 μm and an average content of 15.25%. A tiny amount of mica can be found suspended in clay materials (Fig. 7D).

4.2.5. *Massive carbonate-bearing siliceous siltstones (RT5)*

RT5 is mainly distributed in the middle and lower part of the Wufeng Formation, with a silty texture and gray to grayish-white color (Fig. 6A1). Felsic minerals are the dominant mineral components of detrital grains (Fig. 6A2), with an average content of 54.63%. The particles are mostly 25–60 μm in diameter, a few of which are up to 100 μm, angular to sub-angular. The carbonate minerals are mainly dolomite and calcite (Table 2). The calcite has an average content of 11.60% and a particle size less than 40 μm, with sub-angular grains. The dolomite mainly exists as well idiomorphic crystal grains, and the average content of dolomite is 10.70%, and the diameter of the idiomorphic particles is 70–150 μm. There is a small amount of mica in short and thin strip shapes, with a particle length of 40–120 μm; it is randomly distributed between quartz and feldspar grains (Fig. 6A3), with a content of less than 5.00%. Bioturbation structures are occasionally developed, where locally enriched quartz, feldspar, and calcite grains are cemented by micritic dolomite into clusters, shown as white irregular spots with a diameter of 200–700 μm. These structures indicate frequent biological activities, a shallow water depth, and intense terrestrial input during deposition (Fig. 7E).

4.2.6. *Laminated siliciclastic limestones (RT6)*

RT6 is less distributed, and their OM content is low. They are characterized by pale yellow to pure white bands on the core, forming a lamina assemblage with the clay-rich laminae (Fig. 6B1). Their main component is calcite, whose content is approximately 62.00% (Fig. 6B2). The calcite layers are formed parallel to the laminae (Fig. 6B3), composed of columnar calcite with suitable crystalline form and high purity. The layers are 70–250 μm thick, intercalated with argillaceous clasts, and surrounded by many calcite grains that are sub-angular to sub-rounded and less than 50 μm in diameter (Fig. 7F). The dolomite content is about 5.50%, and the dolomite crystals are well idiomorphic. The following abundant components are clay minerals and detrital quartz. The clay mineral content is about 16.10%. The quartz particles have a diameter of less than 30 μm and a content of roughly 10.20%; they are sub-angular to sub-rounded. A small amount of pyrite is also present, albeit randomly distributed.

4.2.7. *Massive clayey shell limestones (RT7)*

RT7 is developed in the Guanyinqiao Member at the top of the Wufeng Formation (Fig. 6C1), indicating intense biochemical effects. The Hirnantia shells developed during the Hirnantian glaciation are abundant in this strata (Fig. 6C2). These rocks have a gray to grayish-white color, marking the boundary between the Wufeng Formation and the Longmaxi Formation. The dominant mineral component is calcite (Fig. 6C3), whose particles maintain the residual shapes of the shells. The following abundant minerals are quartz and clay minerals. A small amount of dolomite developed with a suitable crystalline form. Some pyrite particles also developed (Fig. 7G), with grain sizes less than 30 μm.

4.2.8. *Massive carbonate-bearing felsic claystone (RT8)*

RT8 is distributed at the bottom of the Wufeng Formation with a small amount (Fig. 6D1). The core shows a grayish-white color, and the OM content is low. The dominant mineral component is clay minerals (Fig. 6D2), with a content of around 46.90%. The detrital materials are evenly distributed among the clay minerals (Fig. 6D3), with a relatively low content of about 28.50%. They are mainly quartz, whose particle size is less than 40 μm. A small amount of carbonate minerals and feldspar is also present, whose particle sizes are all less than 30 μm

(Fig. 7H).

In addition, a small amount of bentonite is frequently developed in the lower part of the WF-L Fm, which thins and shows up less frequently upward. Its dominant mineral compositions are clay minerals and pyrite. Pyrite is densely distributed throughout the bentonite layer (Fig. 7I), giving the entire stratum a golden yellow color distinct from the upper and lower shales. The particle size of pyrite is generally less than 30 μm. In general, the rock types variations in the lower part of the WF-L Fm in the well L204 are more frequent than in the upper part. From bottom to top, the content of detrital grains decreases, and the content of clay minerals increases. The OM content is higher at the bottom than at the top; this shows that the sedimentary environments of the bottom of the WF-L Fm was frequently changing, resulting in frequent variations in rock types.

4.3. Geochemical characteristics

The results show that TOC content of WF-L Fm shales samples ranges from 0.68% to 5.48% (average: 3.31%), mainly concentrated in the range of 1.32%–4.43%. TOC always shows an upward trend, and then shows a downward trend, from the highest value of 5.48%–0.80% (Fig. 8). The variation trend of Cu and Mo content was consistent with TOC. The content of Sr ranged from 94.90 ppm to 325 ppm (average: 181.46 ppm), and the changing trend of Sr content and Sr/Cu ratio was similar. The bottom of WF-L Fm showed an upward trend, then decreased, and then decreased rapidly after a short upward trend, and then kept a low level (Fig. 8). Sr/Ba ratio is between 0.05 and 0.34 (average: 0.11), which is generally at a low level, and its variation trend is similar to that of Sr/Cu. U/Th ratios ranged from 0.17 to 3.00 (average: 1.09), V/Cr ratios ranged from 1.25 to 5.44 (average: 2.52), V/Ni ratios ranged from 0.99 to 3.19 (average: 2.12), and Ni/Co ratios ranged from 2.86 to 29.57 (average: 7.69). The U/Th, V/Cr, V/Ni and Ni/Co change trends are similar. On the whole, WF-L Fm shows an upward trend, and then shows a downward trend (Fig. 8). The content of carbonate minerals slightly decreases upward with minor changes, consistent with the variations of $\delta^{13}C$. The plagioclase content is upwardly increasing, and a small amount of potassium feldspar is present in the upper part. The pyrite content has minor changes, with a stable overall distribution trend.

5. Discussions

5.1. Sedimentary environments evolution

Using geochemical elements and characteristic element ratios as indicators to distinguish paleo-sedimentary environments is a common method for studying fine-grained sedimentary rocks. Cu in water body is easy to combine with OM and deposit to the seafloor, and Mo is easy to enter the sediment in sulfide environments and its deposition flux is proportional to the accumulation rate of OM. When organisms flourish, they preferentially use ^{12}C, resulting in the relative enrichment of ^{13}C in nature and positive excursion of $\delta^{13}C$. Therefore, the Cu content, Mo content, $\delta^{13}C$ and TOC are applied to evaluate the paleoproductivity comprehensively (Calvert and Pedersen, 1993; Lyons et al., 2003; Shen et al., 2011); Sr is precipitated to the water bottom in large quantities under dry conditions, while Cu is deposited rapidly under wet conditions, so that Sr content and Sr/Cu are used to determine paleoclimate (Nesbitt and Young, 1982; Li et al., 2019; Wang et al., 2022a); Both Sr and Ba can enter the water in the form of soluble salts and are sensitive to paleosalinity changes, while Ba^{2+} has a lower solubility than Sr^{2+}, so Ba^{2+} will precipitate before Sr^{2+}, and Sr^{2+} will precipitate when the salinity increases further, making Sr/Ba suitable for judging paleosalinity (Yan et al., 2012; Liang et al., 2017; Li et al., 2020); U, Co, V, Ni and Cr are often enriched in black shale formed under anoxic environments, while Th is not affected by redox conditions. Therefore, the element ratios of U/Th, V/Cr, V/Ni, and Ni/Co can be used to measure redox conditions (Kimura and Watanabe, 2001; Algeo et al., 2011; Algeo et al., 2016; Liu et al., 2019; Algeo and Li, 2020a; Algeo and Liu, 2020b). Based on the above geochemical indicators and the rock types, we analyzed the sedimentary environments in the southern Sichuan Basin (Fig. 8). We divided the evolution process of the sedimentary environments of the Well L204 into 7 intervals, including 3 intervals corresponding to the Wufeng Formation and 4 intervals corresponding to the Longmaxi Formation.

Interval I is 3851.80–3847.30 m. In this interval, the Sr content is low, Sr/Cu < 5, Sr/Ba is relatively low, U/Th < 1, V/Cr is 1.3–2.1, V/Ni is relatively low, and the $\delta^{13}C$, the Cu content and TOC are relatively high. The climate was warm and humid, with high oxygen content in the water body. The sedimentary environments were relatively oxidizing. The paleosalinity declined first and then rose but generally stayed at a low level. TOC remained at a high level, implying high productivity. The rock types are dominantly RT2, RT4, and RT5, with a small amount of RT3 and RT8. In this interval, the clay mineral content is high in the rock type combination, the clastic content is low, and massive structures are developed, indicating a weak hydrodynamic condition. The sedimentation was dominated by the suspension effect. The OM was preserved, and the shales show a dark color.

Interval II is 3847.30–3844.20 m. In this interval, the Sr content increased; Sr/Cu is 3.2–9.1, larger than in Interval I; Sr/Ba >0.3, a high level; U/Th > 1.25; Ni/Co > 6; V/Cr is 2.64–3.57, higher than Interval I; and the Mo content, Cu content and TOC decrease first and then increase, the $\delta^{13}C$ also has a positive excursion, generally at a relatively high level. The climate during this period was relatively hot and dry, the water body was in hypoxic-anoxic conditions, and the paleosalinity was high. The dominant rock type is RT1 interbedded with a small amount of RT3 and RT6. The terrigenous detrital materials increased first and then decreased. The water body temporarily became shallower, and the OM was damaged, resulting in the low TOC value. Large quantities of nutrient elements conducive to the bloom of organisms entered the water body. Thus, microorganisms such as algae flourished, productivity increased, and the OM was enriched, leading to a high Mo content and TOC value.

Interval III is the Guanyinqiao Member between 3844.20 and 3843.10 m. This period was during the Hirnantian glaciation when the climate was cold and dry. The water body became shallow, and organisms such as the *Hirnantia* shells were prosperous; the productivity was high, but the water body was highly oxidizing, damaging the OM and lowering the TOC value. Additionally, the biochemical effects were intense, and RT7 was developed.

Interval IV is 3843.10–3839.00 m, entering the Rhuddanian period. The Sr content and Sr/Cu value are relatively high; Sr/Ba has a declining trend, roughly at a relatively high level; U/Th > 1.25; Ni/Co > 7; V/Cr is 2.7–3.7, at a relatively high level; the content of Cu and Mo is high to low, the TOC is about 4%, and $\delta^{13}C$ has a negative excursion. These factors indicate that the climate was relatively dry and hot. The water body was in anoxic-hypoxic conditions, with large water depth and relatively high productivity. The rock type developed was mainly RT4, with a small amount of RT1 and RT2. The hydrodynamics were weak, and the sedimentation was dominated by the suspension effect.

Interval V is 3839.00–3827.30 m. In this interval, the Sr content and Sr/Cu value decreased, Sr/Ba continually declined, U/Th > 1.25, Ni/Co > 7, V/Cr > 2, and the content of Cu and Mo was generally high, and the $\delta^{13}C$ has a negative excursion. This shows that the climate changed from relatively dry and hot to warm and humid. The water body was in hypoxic-anoxic conditions, the salinity was low, and the water body was relatively closed, with large water depth and weak hydrodynamics. The OM was well preserved, with a TOC value of about 5% and high productivity. The developed rock type was RT4 in the early interval and dominantly RT1 with a small amount of RT2 and RT6 later. In the later interval, the clastic materials dominated by carbonate minerals increased, the terrestrial input was enhanced; however, the sedimentation was still dominated by the suspension effect.

Interval VI is 3827.30–3825.90 m. In this interval, the Sr/Cu value and Sr content increase first and then decrease; Sr/Ba increases to the maximum and then drops. Meanwhile, U/Th < 0.75, Ni/Co < 5, V/Cr < 2, the content of Cu and Mo is relatively low, the TOC has a low value, and the $\delta^{13}C$ shows a strong negative excursion, indicating that the climate was relatively dry and hot during the deposition, the water body became shallower, and the salinity was relatively high. The oxygen content in the water increased, damaging the organic matter, and the TOC declined. The productivity was relatively low. The rock types are mainly RT1 and RT6.

Interval VII is 3825.90–3806.10 m. In this interval, Sr/Cu < 5; the Sr content increases slightly but generally at a low level; Sr/Ba also has a slight increase but is relatively low in general; the indicators, U/Th, Ni/Co, and V/Cr, all have a declining trend, and in general, U/Th < 0.75, Ni/Co < 5, and V/Cr < 2; the content of Cu and Mo gradually decreases; and the TOC continuously decreases from 3.6% to 0.8%. Compared with the Interval VI, the $\delta^{13}C$ have a positive excursion, but still at a lower level. These factors indicate that the climate was warm and humid, and the water body was shallow, with relatively low salinity. The oxygen content of the water was high, and the water body was in a relatively oxidizing condition, where the OM was not easy to preserve. Moreover, the productivity gradually decreased. The water body was poorly closed, with intense terrestrial input. The siliciclastic materials gradually increase upward, their particle size increases, and the rock color becomes lighter. The dominant rock type is RT1, with a small amount of RT5. The sedimentation was dominated by the suspension effect, undersets, and turbidity currents.

In general, Intervals I to VII were dominated by a warm and humid climate, and the paleoclimate experienced an evolution process of warm-humid, relatively hot-dry, cold-dry, hot-dry, warm-humid, relatively hot-dry, and warm-humid. At the same time, the salinity of the water body gradually increased from intervals I to III, generally decreasing trend from intervals IV to VII, only temporarily increasing in Interval VI. The paleo-redox conditions exhibited an evolution trend from relatively oxidizing to anoxic from Intervals I to IV. Except for Interval III during the Hirnantian glaciation when the water body became shallow and oxidizing, there was a hypoxic-anoxic environment with large water depth from intervals II to V. From intervals VI to VII, the water became shallower, showing a relatively oxidizing environment. The paleoproductivity was at a high level from intervals I to V, with a high TOC content. From intervals VI to VII, the paleoproductivity decreased, with only a slight increase at the beginning of Interval VII.

5.2. Impacts of different geological events

5.2.1. Environmental response

The frequent global geological events in late Ordovician to early Silurian had a great impact on the sedimentary environments of shales and the accumulation of OM. In the sedimentary environments evolution of Well L204, from interval I to II, the U/Th ratio rises from 0.17 to 1.40, the V/Cr ratio rises from 1.27 to 3.57, the V/Ni ratio rises from 0.99 to 3.19, and the Ni/Co ratio rises from 3.28 to 10.11, all indicating that the sedimentary environments have changed to anoxic reduction environments. The $\delta^{13}C$ decrease from −0.90‰ to −15.20‰, this is because the reduction of ^{12}C absorbed by OM leads to the relative deficit of ^{13}C in the natural carbon pool, which leads to the negative excursion of $\delta^{13}C$ (Kump and Garrels, 1986; Berner, 1987). Meanwhile, the contents of Cu and Mo also increased, and TOC increased from 0.68% to 5.18%, indicating that marine productivity was also on the rise. These changes may be related to the intense volcanic activity during the sedimentary period of Wufeng Formation from interval I to II. The volcanic eruption of gas contains a large amount of gases such as CO_2, N_2, and NO_2, promoting carbon, nitrogen, and other nutrients in ocean circulation (Olgun et al., 2013; Wu et al., 2018; Zhang et al., 2021; Lu et al., 2022; Yang et al., 2022). Volcanic ash falls into the ocean and hydrolyzes, causing Fe, Cu, and other nutrients and part of SiO_2 to dissolve into water, creating good conditions for sea creatures to flourish (Duggen et al., 2007; Langmann et al., 2010; Xiao et al., 2021; Lu et al., 2022). The gases such as SO_2 and H_2S emitted by volcanoes form acid rain in the stratosphere and then fall into the ocean, resulting in sulfurized anoxia in water bodies (Haeckel et al., 2001; Hammarlund et al., 2012; Cooper et al., 2018; Zhang et al., 2021). A large amount of gas sprayed out in a volcanic activity forms an aerosol through a photochemical reaction in the stratosphere (Robock and Matson, 1983; Robock, 2000; Self et al., 2014). The aerosols can spread globally in a short time and remain suspended in the atmosphere for 1–2 years, Aerosols and volcanic ash work together to reflect some of the solar radiation back into space before they reach the surface, causing the surface to receive less solar radiation and thus lower surface temperatures (Oman et al., 2005; Watson et al., 2017; Cooper et al., 2018; Wang et al., 2019a). This effect inhibits the growth of biological reproduction and reduces productivity, coupled with a cooling of the surface that promotes glaciation, which may have contributed to the first pulse of the Late Ordovician mass extinction (LOME-1) (Chen et al., 2004; Jones et al., 2017; Zou et al., 2018; Hu et al., 2020; Lu et al., 2021).

Interval III is in Hirnantian glaciation, cold water of benthic *Hirnantia* fauna creatures flourish, productivity rising, and RT7 development. The Hirnantian glaciation led to global regression and a significant drop in sea level, rising water salinity, and the cold and dry climate favors carbonate mineral deposits (Yan et al., 2012; Jin et al., 2020; Chen et al., 2021). In Interval IV, the U/Th ratio, V/Cr ratio, and Ni/Co ratio reached the highest value of 3.00, 5.43, and 29.57, after the end of the Hirnantian glaciation, indicating that the sedimentary environments were in the state of deep water and extreme hypoxic reduction, and TOC also reached 4.33%. At the end of the late Hirnantian glacial period, the glaciers rapidly melted and injected a large amount of fresh water into the ocean, resulting in a wide range of transgression and the rapid rise of sea level. Water salinity decreased and water depth increased, resulting in water hypoxia (Jones et al., 2017; Zou et al., 2018; Wu et al., 2019b; Lu et al., 2021). The rapid rise and fall of sea level caused seriously disturbed the stability of the ecosystem, leading to the mass death of organisms represented by the *Hirnantia* fauna, resulting in the second pulse of Late Ordovician mass extinction (LOME-2) (Sheehan, 2001; Hammarlund et al., 2012; Wang et al., 2019a).

5.2.2. Sediment deposition rate

By analyzing the geochemical characteristics and mineral characteristics can be concluded that Interval VII mainly develops RT1 with low TOC content. RT1 presents rich-clay laminae and clastic particles interbed characteristics, rich-clay laminae often appear larger felsic mass particles. It shows that the hydrodynamic force was strong when RT1 was deposited. The climate was warm and humid with strong weathering and terrigenous input, thus accelerated deposition rate and diluted OM in Interval VII. Meanwhile, the water body present an oxidation environment, and the deposited OM is destroyed, resulting in a low TOC content. The main rock types of Interval III and Interval IV are RT7 and RT6, with low TOC content. Interval III was in the Hirnantian Glaciation, the cold and dry climate weakened the weathering greatly, the deposition rate decreased and the OM was oxidized due to the shallow water, so the TOC content of RT7 formed at this time was low. The rock types developed from Interval I to II and from Interval IV to V mainly developed RT2 and RT4, with high TOC content and massive structure, indicating that the sedimentary environments were in a long-term stable state, with weak hydrodynamics and stable deposition rate. Large water depth resulted in low oxygen content in the water, which was conducive to the preservation of OM.

From Interval I to V, high productivity, the anoxic reductive environments formed by large water depth, and a stable deposition rate make the OM well preserved, which is conducive to the development of organic-rich shales. High-quality organic-rich shales are often developed in deep water reductive environments that are conducive to OM

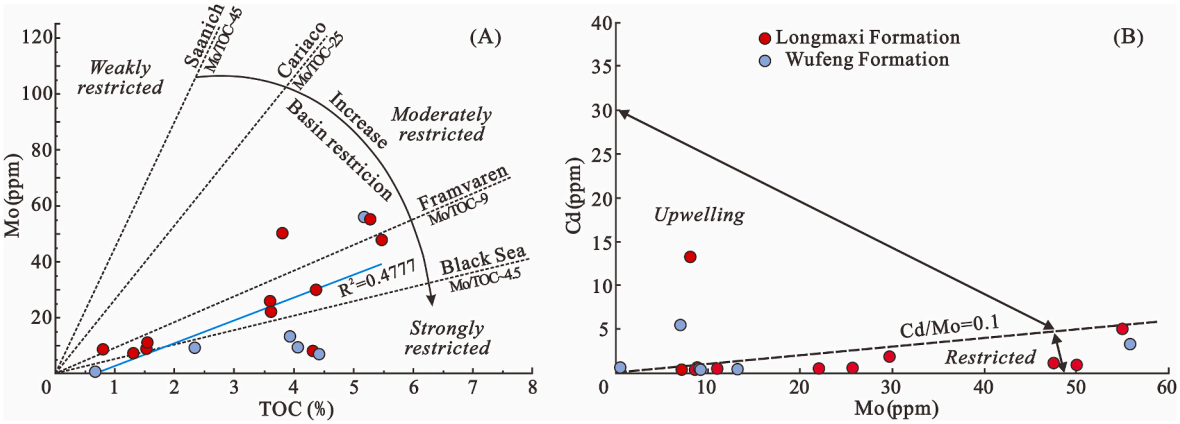

Fig. 9. Plot of TOC versus Mo of WF-L Fm and Plot of Mo versus Cd of WF-L Fm in the study area The Mo/TOC regression lines are from modern environments (Algeo and Lyons, 2006; Algeo and Rowe, 2012). The inferred thresholds for Mo–Cd graphs are based on modern settings (Sweere et al., 2016).

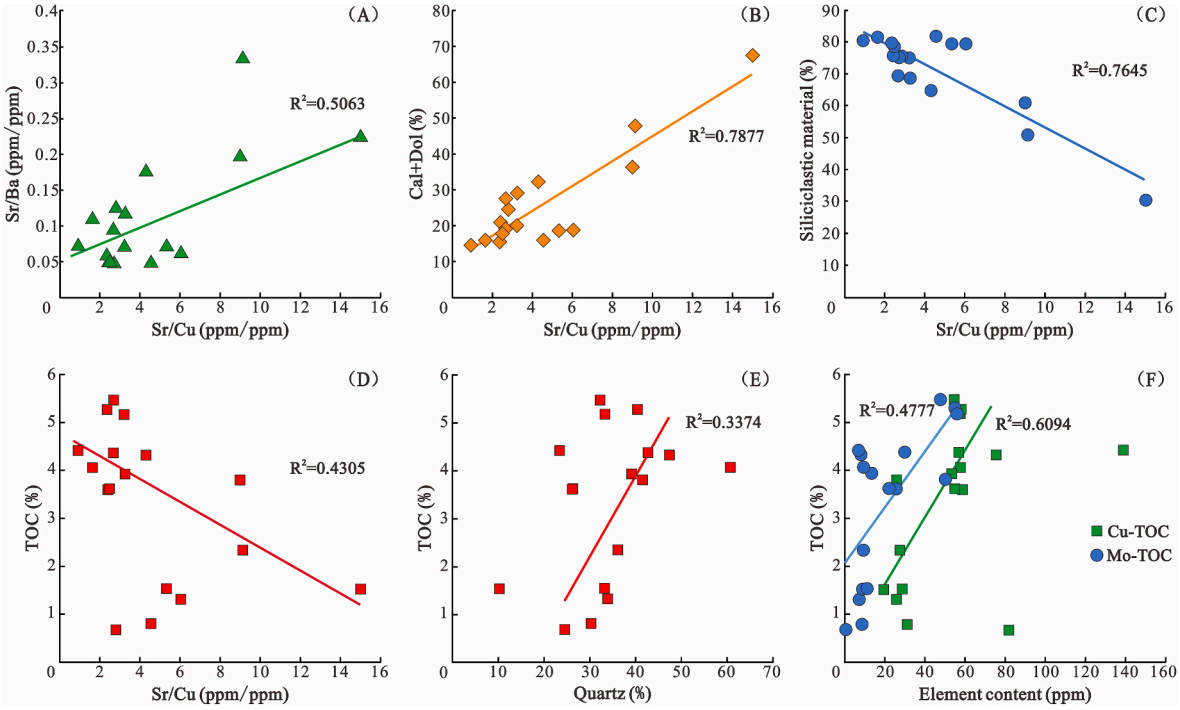

Fig. 10. Trace elements content and ratios, mineral content, and TOC rendering map in the study area.

accumulation and preservation, but the gravity flows can carry organic debris from shallow water into deep water, as well as the surface of terrigenous clastic and oxygen into deep waters, accelerate deposition rate and change the deep-water area's stable anoxic environments, have certain destruction of OM (Ghadeer and Macquaker, 2012; Li et al., 2020; Feng et al., 2021).

The Mo/TOC ratio and Cd/Mo ratios are used to assess the degree of restriction of the water body (Algeo and Lyons, 2006; Algeo and Rowe, 2012; Sweere et al., 2016; Lu et al., 2020). In the study area, Mo/TOC ratio of the Wufeng Formation shales samples is between 0.8 and 10.76 (average: 3.80), Mo/TOC ratio of the Longmaxi Formation sample is between 1.88 and 13.15 (average: 7.57) (Fig. 9A), and 3 samples have Cd/Mo ratios larger than the 0.1 threshold (Fig. 9B), which indicate that the restrictions of the water body from the Wufeng Formation to Longmaxi Formation have weakened, and it is affected by upwelling. The upper part of the Interval II has the upwelling, and a large number of algae and radiolarians can be seen in the development of RT3, which provides a rich OM. TOC increased from 2.34% to 5.18%, indicating that organisms flourished, productivity increased, and OM accumulation. The upwelling current brings a lot of nutrients from deep water to the surface of the water body, enhances the flux of surface nutrients and promotes the increase of primary productivity, thus accelerate deposition rate of OM (Anderson et al., 2009; Scholz et al., 2011; Yang et al., 2021).

5.3. Accumulation process of OM

OM accumulation is mainly controlled by productivity, preservation conditions, and deposition rate, of which productivity and preservation conditions are mainly affected by environmental factors such as climate and reducibility.

The higher Sr/Cu ratio, the drier climate, and the higher Sr/Ba, the higher salinity of water (Liang et al., 2017; Li et al., 2019; Wang et al., 2022a). Based on the analysis of rock type evolution and sedimentary environments in southern Sichuan Basin, we find that Sr/Cu and Sr/Ba are positively correlated (Fig. 10A), while Sr/Cu and carbonate mineral

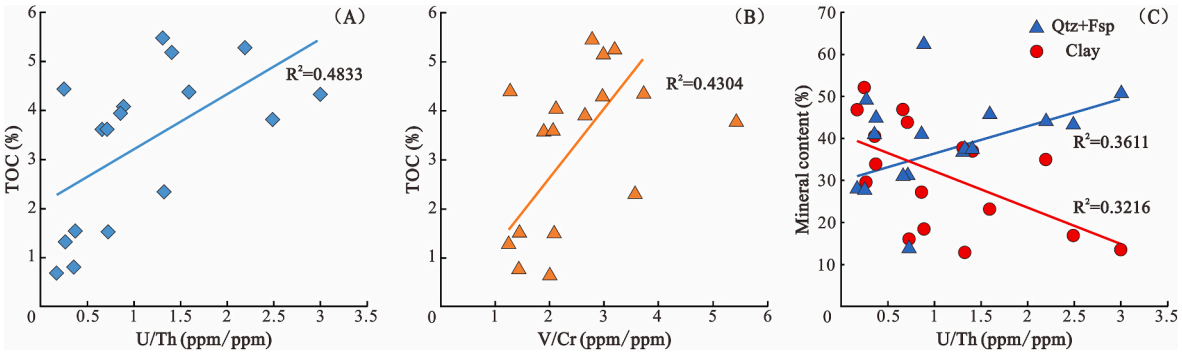

Fig. 11. Trace elements ratio, mineral content and TOC rendering map in the study area.

content are positively correlated (Fig. 10B), Sr/Cu and the siliciclastic material content are negatively correlated (Fig. 10C). It indicate that compared with the warm and humid climate, the dry and hot climate can improve the salinity of water, which is conducive to the development of carbonate minerals and the reduction of siliciclastic material. Meanwhile, Sr/Cu and TOC are negatively correlated (Fig. 10D), TOC and quartz content are positive correlation (Fig. 10E), indicating that a dry and hot climate will lead to a significant decrease in TOC and quartz content. From Intervals IV to VII, the climate changed from warm and humid to dry and hot, the quartz content decreased (Fig. 3), productivity decreased, and TOC decreased gradually (Fig. 8).

Mo content and Cu content are proportional to the level of primary productivity (Lyons et al., 2003; Shen et al., 2011). In Fig. 10F, Mo content and TOC are positively correlated, while Cu content and TOC are positively correlated, indicating that the higher the marine primary productivity is, the higher the TOC is in the sedimentary rocks formed (Fig. 10F). The OM content is generally high in the fine-grained sedimentary rocks of the WF-L Fm in the study area. The rocks have dark colors, indicating that a large quantity of inorganic carbon in the paleo-ocean was converted into organic carbon during the development of the fine-grained rocks. Organisms flourished in the surface seawater, with relatively high productivity. For instance, from Intervals I to II, the paleoproductivity had an overall increasing trend, and the RT3 is frequently developed, the TOC was relatively high. Interval III was within the Hirnantian glaciation when the cool-water benthic *Hirnantia* fauna was prosperous with high productivity (He et al., 2019; Lu et al., 2019; Jin et al., 2020), and the RT7 was developed. After that, from Intervals IV to V, the paleoproductivity was maintained at a high level, the TOC was relatively high, and the core color was dark. The developed rock type was mainly the RT4. From Intervals VI to VII, the water body became shallow, and the terrestrial input increased. The productivity exhibits a decreasing trend, and the TOC declines continually, the core

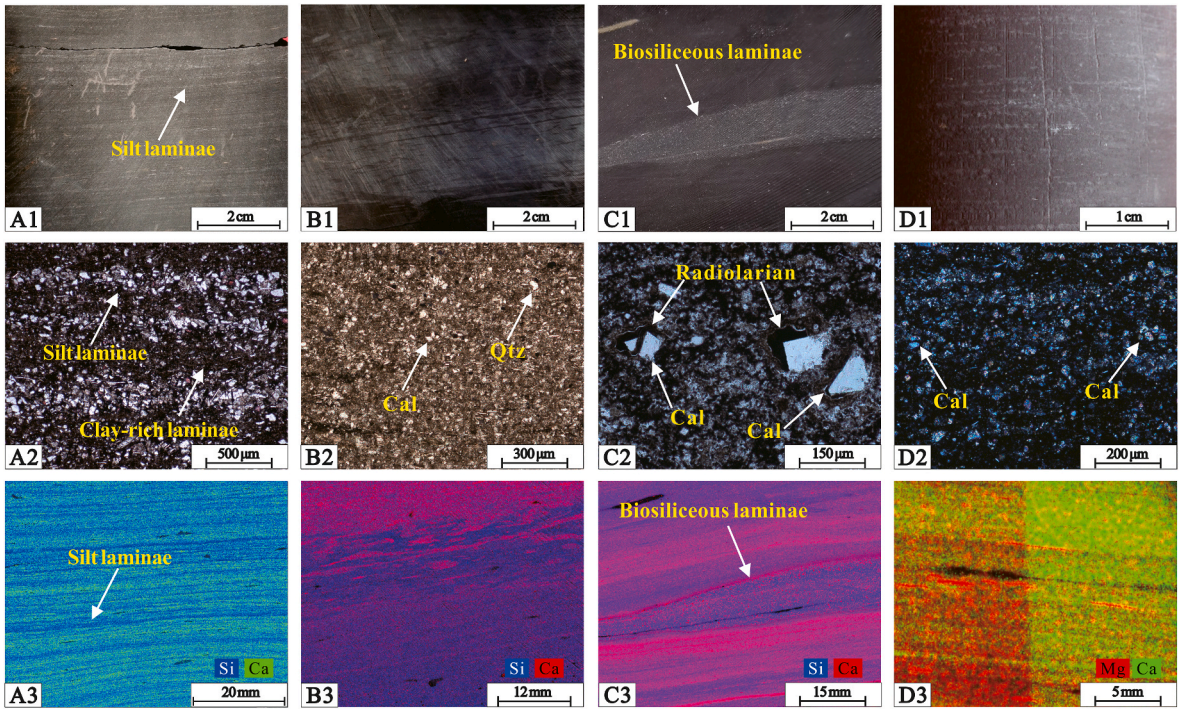

Fig. 5. Characteristics of RT1-RT4 of fine-grained sedimentary rocks in southern Sichuan Basin A-Laminated siliciclastic mixed fine-grained sedimentary rock, A1. Core features, Well L204, 3790.10 m; A2. Microscopic characteristics, Well L204, 3790.22 m, (−); A3. Element distribution of Si and Ca (XRF), Well L204, 3790.17 m; B-Massive siliciclastic mixed fine-grained sedimentary rock, B1. Core features, Well L204, 3851.90 m; B2. Microscopic characteristics, Well L204, 3851.09 m, (−); B3. Element distribution of Si and Ca (XRF), Well L204, 3851.88 m; C-Laminated biosiliceous mixed fine-grained sedimentary rock, C1. Core features, Well L204, 3847.80 m; C2. Microscopic characteristics, radiolarians in the core, Well L204, 3847.70 m, (+); C3. Element distribution of Si and Ca (XRF), Well L204, 3847.80 m; D-Massive calcareous mixed fine-grained sedimentary rocks, D1. Core features, Well L204, 3848.82 m; D2. Microscopic characteristics, Well L204, 3839.34 m, (+); D3. Element distribution of Mg and Ca (XRF), Well N222, 4331.05 m.

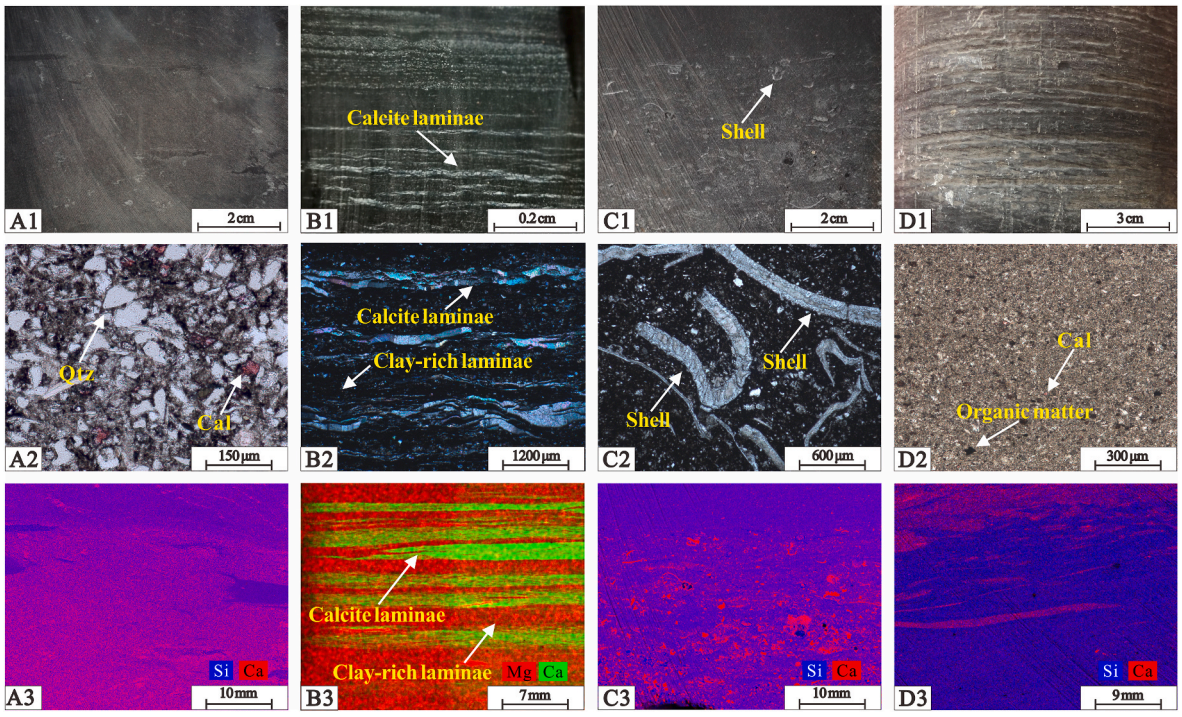

Fig. 6. Characteristics of RT5-RT8 of fine-grained sedimentary rocks in southern Sichuan Basin A-Massive carbonate-bearing siliceous siltstone, A1. Core features, Well L204, 3849.80 m; A2. Microscopic characteristics, Well L204, 3849.85 m, (−); A3.Element distribution of Si and Ca (XRF), Well L204, 3849.80 m; B-Laminated siliciclastic limestone, B1. Core features, Well L204, 3838.40 m; B2. Calcite laminae and clay-rich laminae, Well L204, 3838.40 m, (+); B3. Element distribution of Si and Ca (XRF), well N227, 3598.17 m; C-Massive clayey shell limestone, C1. Core features, Well L204, 3843.20 m; C2. Microscopic characteristics, Well L204, 3843.20 m, (−); C3. Element distribution of Si and Ca (XRF), Well L204, 3843.20 m; D-Massive carbonate-bearing felsic claystone, D1. Core features, Well L204, 3851.93 m; D2. Microscopic characteristics, Well L204, 3851.95 m, (−); D3. Element distribution of Si and Ca (XRF), Well L204, 3851.95 m.

color becomes lighter, and the RT1 is more frequently developed.

The larger the ratio of U/Th and V/Cr, the more the water body is inclined to the anoxic reduction environments (Algeo et al., 2011; Algeo and Li, 2020a; Algeo and Liu, 2020b). We find that U/Th and TOC are positively correlated (Fig. 11A), V/Cr and TOC are positively correlated (Fig. 11B), indicating that the reducing environments are conducive to the preservation of OM. At the same time, there is a negative correlation between U/Th and clay mineral content, and a positive correlation between U/Th and felsic debris content(Fig. 11C), indicating that the rocks formed under reduction environments have a higher content of felsic debris and a lower content of clay material. In the early Rhuddanian period, the earth rapidly entered a greenhouse period (Wu et al., 2019b; Chen et al., 2021; Zhang et al., 2021), and the glaciers melted. The rapidly rising sea level turned the water body into an anoxic environment, where the OM was well preserved. Meanwhile, the water depth was large, and the deposition rate was low. The rock types formed at this time have high TOC, the content of detrital particles is high, and the clay mineral content is relatively low. From Interval II to V, the water body was generally in an anoxic reducing condition, the water depth was large, and the rock types developed were mainly the RT4, with a small amount of RT2; the TOC values are generally high. In Interval I and from Interval VI to VII, the water body was shallow and oxidizing, and the terrestrial input was intense. The clay mineral content is relatively high, and the content of clastic materials is relatively low. The rocks developed are mainly the RT1 and RT5. The corresponding TOC values are relatively low.

5.4. Sedimentary model

The development of the rock types of the WF-L Fm was controlled by multiple factors. The paleoclimate played a decisive role and was interrelated with paleoproductivity and paleo-redox conditions. Sedimentary events such as volcanic activities and the Hirnantian glaciation interrupted the normal deposition process. The gases and ash released by the volcanoes could alter the water environments; the cold and dry climate during the Hirnantian glaciation triggered the first mass extinction in geological history.

In the study area, when the relative strong terrigenous input enters the water body, under the influence of sedimentary differentiation, silt laminae are mainly composed by coarse-grained detrital sediments and clay-rich laminae are mainly composed by clay minerals under suspension, then two laminae interbedded to form RT1 (Fig. 5A; Wang et al., 2019a; Shi et al., 2020). A large number of clay minerals and small-size detrital grains enter the water body and are deposited under suspension to form RT2 (Fig. 5B). Upwelling carries nutrients and dissolved silica to the surface of the water, which promotes the flourishing of surface organisms and the growth of siliceous organisms, so that a large number of siliceous biological shells can overcome the dissolution and settle to the seabed, and are preserved to form RT3 (Fig. 5C; Bolton et al., 2010; Wittke et al., 2010; Liu et al., 2017; Yang et al., 2021). The debris particles in RT4 mainly consist of carbonate particles, quartz, feldspar, indicating RT4 may have been formed by mixed deposition of carbonate rocks debris from Guizhou Uplift and siliceous debris and clay minerals from other provenances (Fig. 5D). The size of the debris in RT5 is generally over 60 μm, and some of the debris is over 100 μm, and the debris is disorderly and the long axis of the particles is not oriented, indicating that the turbidity current brings a large number of debris sediments from shallow water into the deep water and rapidly deposits to form RT5 (Fig. 6A; Liang et al., 2016). The calcite laminae of RT6 may be precipitated by diagenetic fluid intruding into rock fractures (Fig. 6B; Nie et al., 2020; Luo et al., 2021; Wu et al., 2021). RT7 is a kind of shell limestone deposited by the cold-water benthic *Hirnantia* fauna during the Hirnantian glaciation when the glacier developed and the waterbody became shallow (Fig. 6C; Kiipli et al., 2020; Rong et al., 2020; Wang et al., 2022b). RT8 has a very low TOC content (TOC is 0.68% in Well L204, 3851.95 m), which indicates that the deposition rate is fast and

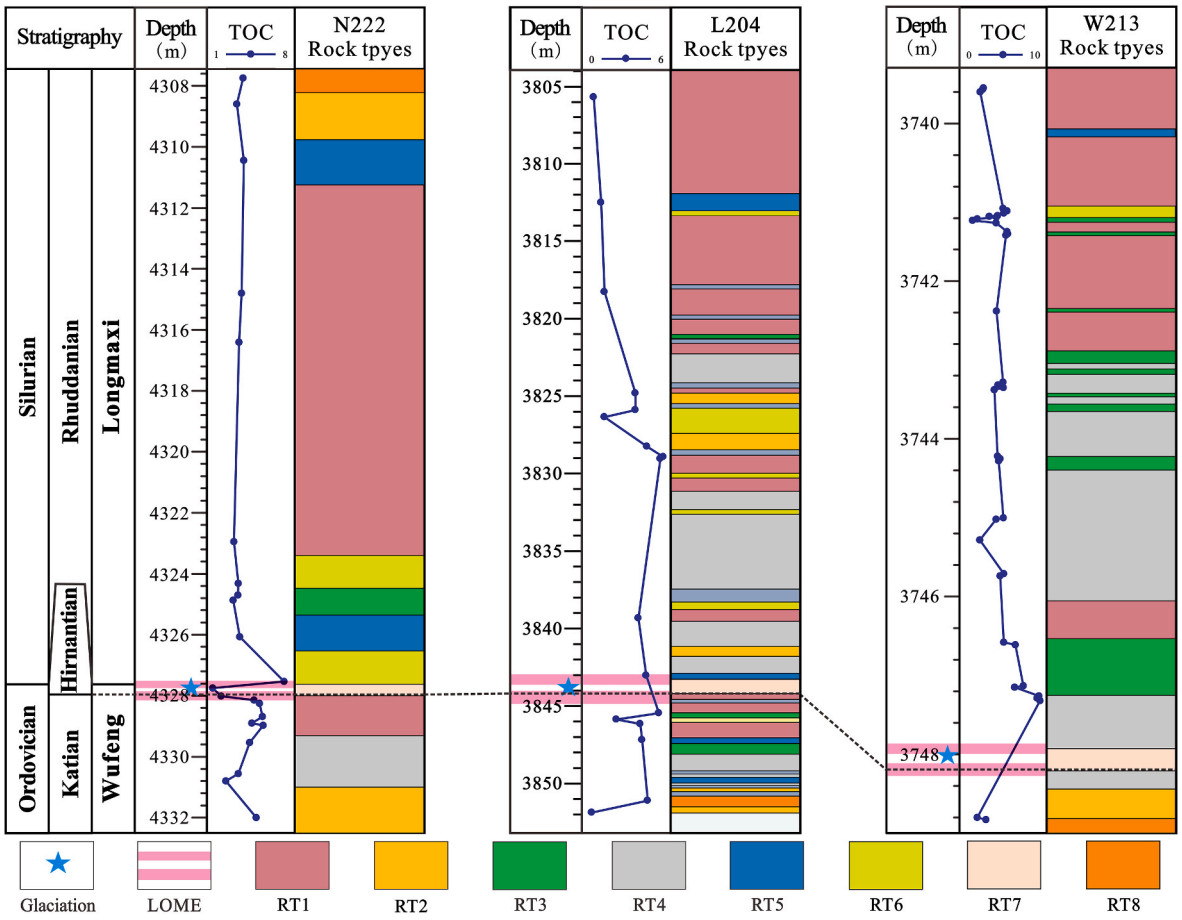

Fig. 12. The geological events and rock types development for the WF-L Fm in southern Sichuan Basin.

the enrichment process is rapid. It may be related to the rise of the early sea level of the Wufeng Formation, a large number of clay minerals and fine-grained debris particles accumulate to form RT8 (Fig. 6D). At the same time, the volcanic ash produced by volcanic activity fall into the ocean through the atmosphere or move through the river, and sedimentation to form bentonite (Fig. 7I; Watson et al., 2017; Plunkett and Pilcher, 2018; Yang et al., 2022).

Through the analysis of the relationship between geological events and rock types development of Well N222, Well L204 and Well W213 in southern Sichuan Basin, it is found that continuous volcanic activity promotes the formation of more anoxic environment in water bodies of the Katian-early Rhuddanian period. The climate is generally in warm and wet environment, and there is also a short dry and hot climate. The salinity of water bodies is at a high level, and the primary productivity is at a high level. RT3, RT4 and a small amount of RT2 were developed, and TOC content was generally high (Fig. 12). More RT7 was developed in dry and cold shallow water during the Hirnantian glaciation. Along with the decrease of sea level in the later Rhuddanian period, the water becomes shallower, the primary productivity decreases, the water oxidizability increases, the terrigenous input increases, the water salinity decreases, the climate tends to warm and wet environment, the main deposits of RT1 and RT5, and the TOC content is generally low. In addition, the formation of RT6 is related to the hydrothermal process. The hydrothermal intrusion along the weak interlaminar surface precipitates columnar calcite, forming columnar calcite layer parallel to the laminar. The bottom of Wufeng Formation in well L204, the top of Longmaxi Formation in well N222 and the bottom of Wufeng Formation in well W213 are all in water environment with strong oxidation, and RT8 with very low TOC content is developed. These results indicate that the geological events of the Late Ordovician-Early Silurian changed the sedimentary environment in southern Sichuan Basin, and then affected the development process and distribution of rock types in the WF-L Fm. The volcanism, glaciation, mass extinction and other geological events occurred in Late Ordovician-Early Silurian have global characteristics, which may mean that the geological events at that time affected the development of rock types all over the world.

We proposed the sedimentary models of the WF-L Fm in the southern Sichuan Basin based on a comprehensive analysis of the rock types characteristics and their assemblages, the evolution of sedimentary environments, the features of sedimentary structures, and mineral component characteristics. During the deposition of the WF-L Fm, the early water body was anoxic and reducing, the water depth was large, and the TOC in the strata was high. The development of the fine-grained sedimentary rocks was controlled by some factors such as the upwelling current, turbidity currents, and suspension sedimentation (Fig. 13). At the same time, irregular volcanic activities also affected the sedimentary environments, and the deposition process of the WF-L Fm shales were jointly controlled by multiple factors.

6. Conclusions

(1) Eight rock types have been identified, and the minerals occurrence model has been thoroughly characterized. The sedimentary environments of the WF-L Fm shales can be further divided into 7 intervals. The results show that Interval I to Interval V represents an anoxic environment with large water depth, high salinity, and high productivity, and Interval VI to Interval VII represents an oxidizing environment with shallow water depth, lower salinity, and lower productivity.

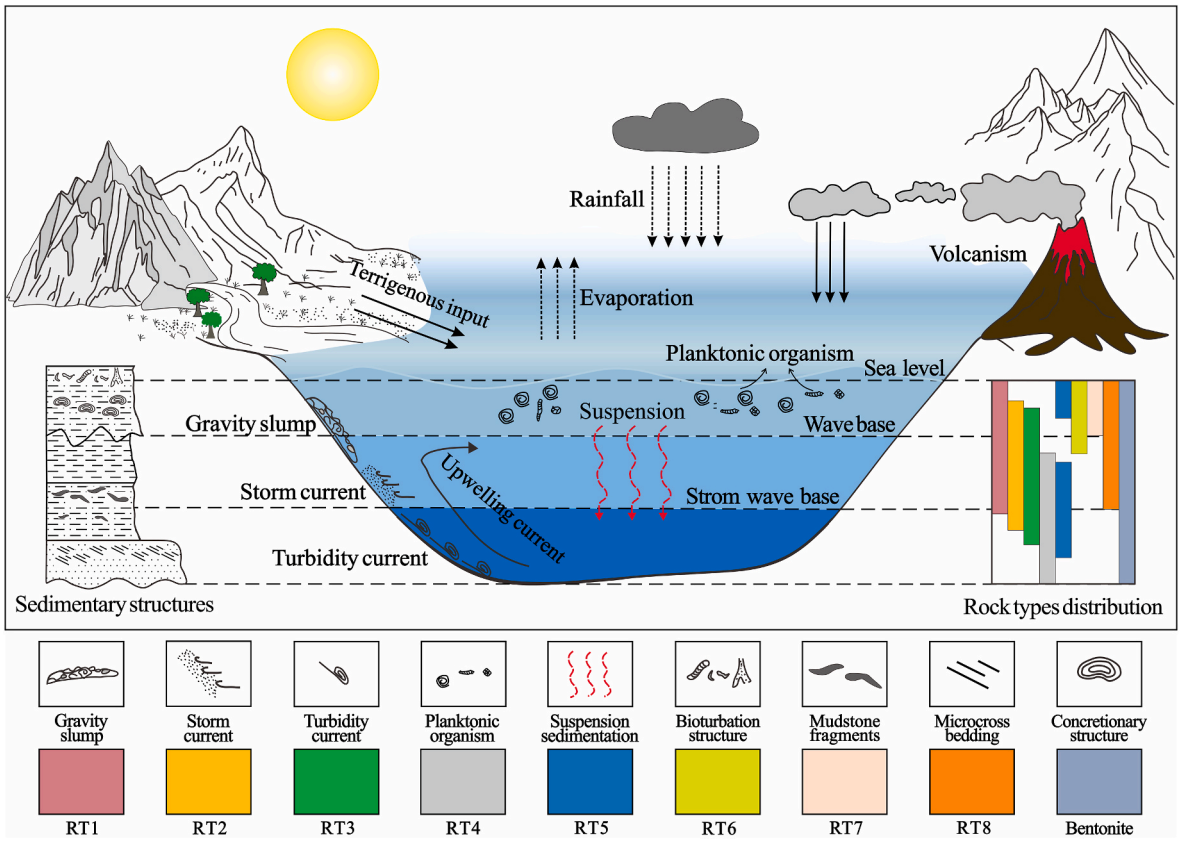

Fig. 13. Conceptual sedimentary model for the WF-L Fm in southern Sichuan Basin.

(2) Palaeoclimate interacted with redox condition, paleosalinity, and paleoproductivity, thus controlling rock types development and OM accumulation. Volcanic activity can make the water body anoxic, and the hydrolysis of the ash releases a lot of nutrients and improves productivity, and is beneficial to the accumulation and preservation of OM. The rapid rise and fall of sea level caused by the Hirnantian glaciation disturbed the stability of the ecosystem, resulting in mass extinctions and providing material sources for OM accumulation. Gravity flow can enhance terrigenous input in deep water for a short time, accelerate deposition rate and dilute OM. The upwelling current enhances nutrient flux in surface water and improves the primary productivity of water, thus affecting the development of WF-L Fm shales.

(3) The development of rock types is the result of the interrelationship between a stable sedimentary environment and sudden geological events. In a given time interval, geological events can also play a leading role in the formation of rock types.

(4) This study reveals the influence mechanism of geological events on the formation of complex rock types and the OM accumulation in Late Ordovician-Early Silurian, southern Sichuan Basin, which provides a comparison of environmental impact mechanisms of geological events occurring in different regions at different periods. Meanwhile, this study clarifies the impacts of geological events on ecological environments, and it is significant to elucidate the global environmental impacts of geological events occurring today.

Declaration of competing interest

The authors declare that they have no known competing financial interests or personal relationships that could have appeared to influence the work reported in this paper.

Data availability

Data will be made available on request.

Acknowledgments

The work presented in this paper was supported by the National Natural Science Foundation of China (No.41902134 and No.42172165), Taishan Scholars Program (No.TSQN201812030). Meanwhile, we are deeply grateful to editors and reviewers for their excellent work and constructive suggestions.

References

Algeo, T.J., Lyons, T.W., 2006. Mo-total organic carbon co-variation in modern anoxic marine environments: implications for analysis of paleoredox and paleohydrographic conditions. Paleoceanography 21, 16–23.

Algeo, T.J., Kuwahara, K., Sano, H., Bates, S., Lyons, T., Elswick, E., Hinnov, L., Ellwood, B., Moser, J., Maynard, J.B., 2011. Spatial variation in sediment fluxes, redox conditions, and productivity in the Permian-Triassic Panthalassic Ocean. Palaeogeogr. Palaeoclimatol. Palaeoecol. 308, 65–83.

Algeo, T.J., Rowe, H., 2012. Paleoceanographic applications of trace-metal concentration data. Chem. Geol. 324–325, 6–18.

Algeo, T.J., Marenco, P.J., Saltzman, M.R., 2016. Co-evolution of oceans, climate, and the biosphere during the "Ordovician Revolution": a review. Palaeogeogr. Palaeoclimatol. Palaeoecol. 458, 1–11.

Algeo, T.J., Li, C., 2020a. Redox classification and calibration of redox thresholds in sedimentary systems. Geochem. Cosmochim. Acta 287, 8–26.

Algeo, T.J., Liu, J.S., 2020b. A re-assessment of elemental proxies for paleoredox analysis. Chem. Geol. 540, 1–12.

Anderson, R.F., Ali, S., Bradtmiller, L.I., Nielsen, S.H.H., Fleisher, M.Q., Anderson, B.E., Burckle, L.H., 2009. Wind-driven upwelling in the southern ocean and the deglacial rise in atmospheric CO_2. Science 323 (5920), 1443–1448.

Berner, R.A., 1987. Models for carbon and sulfur cycles and atmospheric oxygen: application to Paleozoic geologic history. Am. J. Sci. 287 (3), 177–196.

Bolton, C.T., Lawrence, K.T., Gibbs, S.J., Wilson, P.A., Cleaveland, L.C., Herbert, T.D., 2010. Glacial-interglacial productivity changes recorded by alkenones and microfossils in late Pliocene eastern equatorial Pacific and Atlantic upwelling zones. Earth Planet Sci. Lett. 295, 401–411.

Brenchley, P.J., Carden, G.A., Hint, L., Kaljo, D., Marshall, J.D., Martma, T., Meidla, T., Nõlvak, J., 2003. High-resolution stable isotope stratigraphy of Upper Ordovician sequences: constraints on the timing of bioevents and environmental changes associated with mass extinction and glaciation. Geol. Soc. Am. Bull. 115, 89–104.
Calvert, S.E., Pedersen, T.F., 1993. Geochemistry of recent oxic and anoxic sediments: Implications for the geological record. Mar. Geol. 113, 67–88.
Chen, X., Rong, J.Y., Li, Y., Boucot, A.J., 2004. Facies patterns and geography of the Yangtze region, south China, through the ordovician and silurian transition. Palaeogeogr. Palaeoclimatol. Palaeoecol. 204, 353–372.
Chen, L., Jiang, S., Chen, P., Chen, X.H., Zhang, B.M., Zhang, G.T., Lin, W.B., Lu, Y.C., 2021. Relative sea-Level changes and organic matter enrichment in the upper ordovician-lower silurian wufeng-longmaxi formations in the central Yangtze area, China. Mar. Petrol. Geol. 124, 1–16.
Cooper, C.L., Swindles, G.T., Savov, I.P., Schmidt, A., Bacon, K.L., 2018. Evaluating the relationship between climate change and volcanism. Earth Sci. Rev. 177, 238–247.
Dong, T., He, S., Chen, M.F., Hou, Y.G., Guo, X.W., Wei, C., Han, Y.J., Yang, R., 2019. Quartz types and origins in the paleozoic Wufeng-Longmaxi Formations, Eastern Sichuan Basin, China: implications for porosity preservation in shale reservoirs. Mar. Petrol. Geol. 106, 62–73.
Duggen, S., Croot, P., Schacht, U., Hoffmann, L., 2007. Subduction zone volcanic ash can fertilize the surface ocean and stimulate phytoplankton growth: evidence from biogeochemical experiments and satellite data. Geophys. Res. Lett. 34 (1), L01612.
Fan, C.H., Li, H., Q, Q.R., He, S., Zhong, C., 2020. Geological conditions and exploration potential of shale gas reservoir in wufeng and longmaxi formation of southeastern sichuan basin, China. J. Petrol. Sci. Eng. 191 (1), 1–16.
Feng, Y.L., Zou, C.N., Li, J.Z., Lin, C.S., Wang, H.J., Jiang, S., Yang, Z., Zhang, S., Fu, X.L., 2021. Sediment gravity-flow deposits in Late Cretaceous Songliao postrift downwarped lacustrine basin, northeastern China. Mar. Petrol. Geol. 134, 1–25.
Feng, Z.Z., 2019. A review on the definitions of terms of sedimentary facies. J. Palaeogeogr. 8 (1), 1–11.
Feng, Z.Z., 2022. Some new thoughts of definitions of terms of sedimentary facies: based on Miall's paper (1985). J. Palaeogeogr. 11 (1), 1–7.
Finnegan, S., Bergmann, K., Eiler, J.M., Jones, D.S., Fike, D.A., Eisenman, I., Hughes, N. C., Tripati, A.K., Fischer, W.W., 2011. The magnitude and duration of late Ordovician-early Silurian glaciation. Science 33, 903–906.
Ge, X.Y., Mou, C.L., Yu, Q., Liu, W., Men, X., He, J.L., 2019. The geochemistry of the sedimentary rocks from the huadi no. 1 well in the wufeng-longmaxi formations (upper ordovician-lower silurian), south China, with implications for paleoweathering, provenance, tectonic setting and paleoclimate. Mar. Petrol. Geol. 103, 646–660.
Ghadeer, S.G., Macquaker, J.H., 2012. The role of event beds in the preservation of organic carbon in fine-grained sediments: analyses of the sedimentological processes operating during deposition of the Whitby Mudstone Formation (Toarcian, LowerJurassic) preserved in northeast England. Mar. Petrol. Geol. 35, 309–320.
Gong, Q., Wang, X.D., Zhao, L.S., Grasby, S.E., Chen, Z.Q., Zhang, L., Li, Y., Cao, L., Li, Z. H., 2017. Mercury spikes suggest volcanic driver of the Ordovician-Silurian mass extinction. Sci. Rep. 7, 1–7.
Haeckel, M., Beusekom, J.V., Wiesner, M.G., König, I., 2001. The impact of the 1991 Mount Pinatubo tephra fallout on the geochemical environment of the deep-sea sediments in the South China Sea. Earth Planet Sci. Lett. 193, 151–166.
Hammarlund, E.U., Dahl, T.W., Harper, D.A.T., Bond, D.P.G., Nielsen, A.T., Bjerrum, C. J., Schovsbo, N.H., Schönlaub, H.P., Zalasiewicz, J.A., Canfield, D.E., 2012. A sulfidic driver for the end-Ordovician mass extinction. Earth Planet Sci. Lett. 331–332, 128–139.
He, L., Wang, Y.P., Chen, D.F., 2019. Geochemical features of sedimentary environment and paleoclimate during late ordovician to early silurian in southern Sichuan Basin. Geochimica 48 (6), 555–566 (in Chinese with English abstract).
Hu, X.T., Chen, L., Qi, L., Lei, Z.A., Luo, Y., 2019. Marine shale reservoir evaluation in the Sichuan Basin-A case study of the Lower Silurian Longmaxi marine shale of the B201 well in the Baoluan area, southeast Sichuan Basin, China. J. Petrol. Sci. Eng. 182, 1–9.
Hu, D.P., Li, M.H., Zhang, X.L., Turchyn, V.A., Gong, Y.Z., Shen, Y.N., 2020. Large mass-independent sulphur isotope anomalies link stratospheric volcanism to the Late Ordovician mass extinction. Nat. Commun. 11, 1–8.
Jiang, Z.X., Tang, X.L., Cheng, L.J., Li, Z., Zhang, Y.Y., Bai, Y.Q., Yuan, Y., Hao, J., 2015. Characterization and origin of the silurian Wufeng-Longmaxi Formation shale multiscale heterogeneity in southeastern Sichuan Basin, China. Interpretation-a Journal of Subsurface Characterization 3 (2), SJ60–SJ74.
Jin, C.S., Liao, Z.W., Tang, Y.J., 2020. Sea-level changes control organic matter accumulation in the Longmaxi shales of southeastern Chongqing, China. Mar. Petrol. Geol. 119, 1–13.
Jones, D.S., Martini, A.M., Fike, D.A., Kaiho, K., 2017. A volcanic trigger for the Late Ordovician mass extinction? Mercury data from south China and Laurentia. Geology 45 (7), 631–634.
Kiipli, E., Kiipli, T., 2020. Hirnantian sea-level changes in the Baltoscandian Basin, a review. Palaeogeogr. Palaeoclimatol. Palaeoecol. 540, 1–13.
Kimura, H., Watanabe, Y., 2001. Oceanic anoxia at the Precambrian-Cambrian boundary. Geology 29, 995–998.
Kump, L.R., Garrels, R.M., 1986. Modeling atmospheric O_2 in the global sedimentary redox cycle. Am. J. Sci. 286 (5), 337–360.
Lambeck, K., Chappell, J., 2001. Sea level change through the last glacial cycle. Science 292 (5517), 679–686.
Langmann, B., Zaksek, K., Hort, M., Duggen, S., 2010. Volcanic ash as fertiliser for the surface ocean. Atmos. Chem. Phys. 10 (8), 3891–3899.
Li, D.L., Li, R.X., Tan, C.Q., Zhao, D., Xue, T., Zhao, B.S., Khaled, A., Liu, F.T., Xu, F., 2019. Origin of silica, paleoenvironment, and organic matter enrichment in the Lower Paleozoic Niutitang and Longmaxi formations of the northwestern Upper Yangtze Plate: significance for hydrocarbon exploration. Mar. Petrol. Geol. 103, 404–421.
Li, L., Liu, Z.J., Sun, P.C., Li, Y.J., George, S.C., 2020. Sedimentary basin evolution, gravity flows, volcanism, and their impacts on the formation of the Lower Cretaceous oil shales in the Chaoyang Basin, northeastern China. Mar. Petrol. Geol. 119, 1–21.
Liang, C., Jiang, Z.X., Yang, Y.T., Wei, X.J., 2012. Shale lithofacies and reservoir space of the Wufeng-Longmaxi Formation, Sichuan Basin, China. Petrol. Explor. Dev. 39 (6), 736–743.
Liang, C., Jiang, Z.X., Cao, Y.C., Wu, M.H., Guo, L., Zhang, C.M., 2016. Deep-water depositional mechanisms and significance for unconventional hydrocarbon exploration: a case study from the lower Silurian Longmaxi shale in the southeastern Sichuan Basin. AAPG (Am. Assoc. Pet. Geol.) Bull. 100, 773–794.
Liang, C., Jiang, Z.X., Cao, Y.C., Zhang, J.C., Guo, L., 2017. Sedimentary characteristics and paleoenvironment of shale in the Wufeng-Longmaxi Formation, north Guizhou province, and its shale gas potential. J. Earth Sci. 28 (6), 1020–1031.
Liu, M., Chen, D.Z., Jiang, L., Stockey, R.G., Aseal, D., Zhang, B., Liu, K., Yang, X.R., Yan, D.T., Planavsky, N.J., 2022. Oceanic anoxia and extinction in the latest Ordovician. Earth Planet Sci. Lett. 588, 1–12.
Liu, Y., Wu, B., Gong, Q.S., Cao, H.Y., 2019. Geochemical characteristics of the lower silurian Longmaxi Formation on the Yangtze Platform, south China: implications for depositional environment and accumulation of organic matters. J. Asian Earth Sci. 184, 1–11.
Liu, Z.H., Algeo, T.J., Guo, X.S., Fan, J.X., Du, X.B., Lu, Y.C., 2017. Paleo-environmental cyclicity in the early Silurian Yangtze Sea (South China): tectonic or glacio-eustatic control? Palaeogeogr. Palaeoclimatol. Palaeoecol. 466, 59–76.
Lu, Y.B., Jiang, S., Lu, Y.C., Xu, S., Shu, Y., Wang, Y.X., 2019. Productivity or preservation? The factors controlling the organic matter accumulation in the late Katian through Hirnantian Wufeng organic-rich shale, South China. Mar. Petrol. Geol. 109, 22–35.
Lu, Y.B., Hao, F., Lu, Y.C., Yan, D.T., Xu, S., Shu, Z.G., Wang, Y.X., Wu, L.Y., 2020. Lithofacies and depositional mechanisms of the Ordovician-Silurian Wufeng-Longmaxi organic-rich shales in the Upper Yangtze area, southern China. AAPG (Am. Assoc. Pet. Geol.) Bull. 104, 97–129.
Lu, Y.B., Hao, F., Yan, D.T., Lu, Y.C., 2021. Volcanism-induced late boda warming in the late ordovician: evidence from the upper Yangtze Platform, south China. Palaeogeogr. Palaeoclimatol. Palaeoecol. 578, 1–13.
Lu, Y.B., Hao, F., Shen, J., Lu, Y.C., Song, H.Y., Wang, Y.X., Gou, Q.Y., 2022. High-resolution volcanism-induced oceanic environmental change and its impact on organic matter accumulation in the Late Ordovician Upper Yangtze Sea. Mar. Petrol. Geol. 136, 1–15.
Luo, T., Guo, X.W., Shu, Z.G., Bao, H.Y., He, S., Qin, Z.J., Gou, Q.Y., 2021. Fluid source and formation time of fracture veins of Wufeng Formation and Longmaxi Formation in the South of jiaoshiba area, Sichuan Basin. Acta Pet. Sin. 42 (5), 611–622 (in Chinese with English abstract)).
Lyons, T.W., Werne, J.P., Hollander, D.J., Murray, R.W., 2003. Contrasting sul-Fur geochemistry and Fe/Al and Mo/Al ratios across the late oxic-to-anoxic transition in the Cariaco Basin,Venezuela. Chem. Geol. 195, 131–157.
Nesbitt, H.W., Young, G.M., 1982. Early proterozoic climates and plate motions inferred from major element chemistry of lutites. Nature 299 (5885), 715–717.
Nie, H.K., He, Z.L., Wang, R.Y., Zhang, G.G., Chen, Q., Li, D.H., Lu, Z.Y., Sun, C.X., 2020. Temperature and origin of fluid inclusions in shale veins of Wufeng-Longmaxi Formations, Sichuan Basin, south China: implications for shale gas preservation and enrichment. J. Petrol. Sci. Eng. 193, 1–18.
Olgun, N., Duggen, S., Andronico, D., Kutterolf, S., Croot, P.L., Giammanco, S., Censi, P., Randazzo, L., 2013. Possible impacts of volcanic ash emissions of Mount Etna on the primary productivity in the oligotrophic Mediterranean Sea: results from nutrient-release experiments in seawater. Mar. Chem. 152 (2), 32–42.
Oman, L., Robock, A., Stenchikov, G., Schmidt, G.A., Ruedy, R., 2005. Climatic response to high-latitude volcanic eruptions. J. Geophys. Res. 110, 1–13.
Plunkett, G., Pilcher, J.R., 2018. Defining the potential source region of volcanic ash in northwest europe during the mid - to late holocene. Earth Sci. Rev. 179, 20–37.
Potter, C.J., 2018. Paleozoic shale gas resources in the Sichuan Basin, China. AAPG (Am. Assoc. Pet. Geol.) Bull. 102, 987–1009.
Qiu, Z., Liu, B., Lu, B., Shi, Z.S., Li, Z.Y., 2022. Mineralogical and petrographic characteristics of the Ordovician-Silurian Wufeng-Longmaxi Shale in the Sichuan Basin and implications for depositional conditions and diagenesis of black shales. Mar. Petrol. Geol. 135, 1–18.
Ran, B., Liu, S.G., Jansa, L., Sun, W., Yang, D., Ye, Y.H., Wang, S.Y., Luo, C., Zhang, X., Zhang, C.J., 2015. Origin of the upper ordovician-lower silurian cherts of the Yangtze block, south China, and their palaeogeo-graphic significance. J. Asian Earth Sci. 108, 1–17.
Robock, A., Matson, M., 1983. Circumglobal transport of the El Chichón volcanic dust cloud. Science 221 (4606), 195–197.
Robock, A., 2000. Volcanic eruptions and climate. Rev. Geophys. 38 (2), 191–219.
Rong, J.Y., Harper, D.A.T., Huang, B., Li, R.Y., Zhang, X.L., Chen, D., 2020. The latest Ordovician Hirnantian brachiopod faunas: new global insights. Earth Sci. Rev. 208, 1–40.
Scholz, F., Hensen, C., Noffke, A., Rohde, A., Liebetrau, V., Wallmann, K., 2011. Early diagenesis of redox-sensitive trace metals in the Peru upwelling area–response to ENSO-related oxygen fluctuations in the water column. Geochem. Cosmochim. Acta 75 (22), 7257–7276.
Self, S., Schmidt, A., Mather, T.A., 2014. Emplacement characteristics, time scales, and volcanic gas release rates of continental flood basalt eruptions on Earth. Geological Society of America special papers 505, 319–337.

Sheehan, P.M., 2001. The Late Ordovician mass extinction. Annu. Rev. Earth Planet Sci. 29, 331–364.
Shen, J., Shi, Z.Y., Feng, Q.L., 2011. Review on geochemical proxies in paleo-productivity studies. Geol. Sci. Technol. Inf. 30 (2), 69–77 (in Chinese with English abstract).
Shi, Z.S., Dong, D.Z., Wang, H.Y., Sun, S.S., Wu, J., 2020. Reservoir characteristics and genetic mechanisms of gas-bearing shales with different laminae and laminae combinations: a case study of Member 1 of the Lower Silurian Longmaxi shale in Sichuan Basin, SW China. Petrol. Explor. Dev. 47 (4), 888–900.
Sweere, T., Boorn, S., Dickson, A.J., Reichart, G., 2016. Definition of new trace-metal proxies for the controls on organic matter enrichment in marine sediments based on Mn, Co, Mo and Cd concentrations. Chem. Geol. 441, 235–245.
Torsvik, T.H., Cocks, L.R.M., 2018. Gondwana from top to base in space and time. Gondwana Res. 24, 999–1030.
Wang, C., Zhang, B.Q., Hu, Q.H., Shu, Z.G., Sun, M.D., Bao, H.Y., 2019. Laminae characteristics and influence on shale gas reservoir quality of lower Silurian Longmaxi Formation in the Jiaoshiba area of the Sichuan Basin, China. Mar. Petrol. Geol. 109, 839–851.
Wang, G.X., Zhan, R.B., Percival, I.G., 2019a. The end-Ordovician mass extinction: a single-pulse event? Earth Sci. Rev. 192, 15–33.
Wang, Y., Liu, L.F., Zheng, S.S., Luoa, Z.H., Sheng, Y., Wang, X.M., 2019b. Full-scale pore structure and its controlling factors of the Wufeng-Longmaxi shale, southern Sichuan Basin, China: implications for pore evolution of highly overmature marine shale. J. Nat. Gas Sci. Eng. 57, 134–146.
Wang, Y.F., Zhai, G.Y., Liu, G.H., Shi, W.Z., Lu, Y.C., Li, J., Zhang, Y.X., 2021. Geological characteristics of shale gas in different strata of marine facies in south China. J. Earth Sci. 32 (4), 725–741.
Wang, Y.C., Ge, X.Y., Mou, C.L., Liang, W., Men, X., 2022a. Sedimentary and geochemical responses to the end ordovician glaciation in the Guanyinqiao formation (late ordovician-early silurian period) in the Sichuan Basin. Geochem. Int. 60, 641–656.
Wang, Y.M., Wang, H.Y., Qiu, Z., Shen, J.J., Zhang, Q., Zhang, L.F., Wang, C.H., Li, X.J., 2022b. Basic characteristics of key interfaces in upper ordovician Wufeng Formation-lower silurian Longmaxi Formation in Sichuan Basin and its periphery, SW China. Petrol. Explor. Dev. 49 (1), 37–51.
Wang, Z.Y., Chen, L., Chen, D.X., Lai, J., Deng, G.S., Liu, Z.Y., Wang, C., 2020. Characterization and evaluation of shale lithofacies within the lowermost longmaxi-wufeng formation in the southeast sichuan basin. J. Petrol. Sci. Eng. 193 (1), 1–10.
Watson, E.J., Swindles, G.T., Savov, I.P., Lawson, I.T., Connor, C.B., Wilson, J.A., 2017. Estimating the frequency of volcanic ash clouds over northern Europe. Earth Planet Sci. Lett. 460, 41–49.
Wittke, F., Kock, A., Bange, H.W., 2010. Nitrous oxide emissions from the upwelling area off Mauritania (NW Africa). Geophys. Res. Lett. 37 (L12601), 1–5.
Wu, L.Y., Lu, Y.C., Jiang, S., Liu, X.F., He, G.S., 2018. Effects of volcanic activities in ordovician wufeng-silurian longmaxi period on organic-rich shale in the upper Yangtze area, south China. Petrol. Explor. Dev. 45 (5), 862–872.
Wu, J., Liang, C., Hu, Z.Q., Yang, R.C., Xie, J., Wang, R.Y., Zhao, J.H., 2019a. Sedimentation mechanisms and enrichment of organic matter in the ordovician wufeng formation-silurian Longmaxi Formation in the Sichuan Basin. Mar. Petrol. Geol. 101, 556–565.
Wu, L.Y., Lu, Y.C., Jiang, S., Liu, X.F., Liu, Z.H., Lu, Y.B., 2019b. Relationship between the origin of organic-rich shale and geological events of the Upper Ordovician-Lower Silurian in the Upper Yangtze area. Mar. Petrol. Geol. 102, 74–85.
Wu, A.B., Cao, J., Zhang, J.K., 2021. Bedding-parallel calcite veins indicate hydrocarbon-water-rock interactions in the over-mature Longmaxi shales, Sichuan Basin. Mar. Petrol. Geol. 133, 1–12.
Wu, B., 2022. The sedimentary geochemical characteristics and geological significance of the Wufeng-Longmaxi Formation accumulation of organic matter black shale on the southeastern Sichuan Basin, China. Geofluids 2022, 1–22.
Xi, Z.D., Tang, S.H., Zhang, S.H., Yi, Y.X., Dang, F., Ye, Y.P., 2019. Characterization of quartz in the wufeng formation in northwest hunan province, south China and its implications for reservoir quality. J. Petrol. Sci. Eng. 179, 979–996.
Xiao, B., Liu, S.G., Li, Z.W., Ran, B., Ye, Y.H., Yang, D., Li, J.X., 2021. Geochemical characteristics of marine shale in the wufeng formation–longmaxi formation in the northern sichuan basin, south China and its implications for depositional controls on organic matter. J. Petrol. Sci. Eng. 203, 1–15.
Yan, D.T., Chen, D.Z., Wang, Q.C., Wang, J.G., 2012. Predominance of stratified anoxic Yangtze Sea interrupted by short-term oxygenation during the OrdoSilurian transition. Chem. Geol. 291, 69–78.
Yan, R.J., Xu, G.S., Xu, F.H., Song, J.M., Yuan, H.F., Luo, X.P., Fu, X.D., Cao, Z.Y., 2022. The multistage dissolution characteristics and their influence on mound-shoal complex reservoirs from the Sinian Dengying Formation, southeastern Sichuan Basin, China. Mar. Petrol. Geol. 139, 1–27.
Yang, C., Li, X.H., Li, Z.X., Zhu, M.Y., Lu, K., 2020. Provenance evolution of age-calibrated strata reveals when and how south China block collided with gondwana. Geophys. Res. Lett. 47 (19), 1–9.
Yang, R., He, S., Wang, X., Hu, Q.H., Hu, D.F., Yi, J.Z., 2016. Paleo-ocean redox environments of the upper ordovician wufeng and the first member in lower silurian longmaxi formations in the jiaoshiba area, Sichuan Basin. Can. J. Earth Sci. 53, 426–440.
Yang, S.C., Hu, W.X., Wang, X.L., 2021. Mechanism and implications of upwelling from the late ordovician to early silurian in the Yangtze region, south China. Chem. Geol. 565, 1–13.
Yang, S.C., Hu, W.X., Fang, J.X., Deng, Y.Y., 2022. New geochemical identification fingerprints of volcanism during the Ordovician-Silurian transition and its implications for biological and environmental evolution. Earth Sci. Rev. 228, 1–18.
Zhang, G.W., Guo, A.L., Wang, Y.J., Li, S.Z., Dong, Y.P., Liu, S.F., He, D.F., Cheng, S.Y., Lu, R.K., Yao, A.P., 2013. Tectonics of South China continent and its implications. Sci. China Earth Sci. 56 (11), 1804–1828.
Zhang, G.Y., Tong, X.G., Xin, R.C., Wen, Z.X., Ma, F., Huang, T.F., Wang, Z.M., Yu, B.S., 2019. Evolution of lithofacies and paleogeography and hydrocarbon distribution worldwide (I). Petrol. Explor. Dev. 46 (4), 664–686.
Zhang, X., Zhang, T.S., Zhao, X.M., Zhu, H.H., Mihai, E.P., Chen, L., Yong, J.J., Xiao, Q., Li, H.J., 2021. Effects of astronomical orbital cycle and volcanic activity on organic carbon accumulation during Late Ordovician-Early Silurian in the Upper Yangtze area, South China. Petrol. Explor. Dev. 48 (4), 850–863.
Zhao, J.H., Jin, Z.J., Jin, Z.K., Hu, Q.H., Hu, Z.Q., Du, W., Yan, C.N., Geng, Y.K., 2017. Mineral types and organic matters of the Ordovician-Silurian Wufeng and Longmaxi Shale in the Sichuan Basin, China: implications for pore systems, diagenetic pathways, and reservoir quality in fine-grained sedimentary rocks. Mar. Petrol. Geol. 86, 655–674.
Zhao, W.Z., Li, J.Z., Yang, T., Wang, S.F., Huang, J.L., 2016. Geological difference and its significance of marine shale gases in South China. Petrol. Explor. Dev. 43 (4), 547–559.
Zhao, G., Jin, Z.J., Ding, W.L., Liu, G.X., Yun, J.B., Wang, R.Y., Wang, G.P., 2022. Developmental characteristics and formational stages of natural fractures in the wufeng - longmaxi formation in the sangzhi block, hunan province, China: insights from fracture cements and fluid inclusions studies. J. Petrol. Sci. Eng. 208, 1–20.
Zhu, Y.Q., Chen, G.S., Liu, Y., Shi, X.W., Wu, W., Luo, C., Yang, X., Yang, Y.R., Zou, Y.H., 2021. Sequence stratigraphy and lithofacies paleogeographic evolution of katian stage-aeronian stage in southern Sichuan Basin, SW China. Petrol. Explor. Dev. 48 (5), 974–985.
Zou, C.N., Dong, D.Z., Wang, S.J., Li, J.Z., Li, X.J., Wang, Y.M., Li, D.H., Cheng, K.M., 2010. Geological characteristics and resource potential of shale gas in China. Petrol. Explor. Dev. 37 (6), 641–653.
Zou, C.N., Qiu, Z., Poulton, S.W., Dong, D.Z., Wang, H.Y., Chen, D.Z., Lu, B., Shi, Z.S., Tao, H.F., 2018. Ocean euxinia and climate change “double whammy” drove the Late Ordovician mass extinction. Geology 46 (6), 535–538.